PHYSICAL ADSORPTION OF ARGON, KRYPTON AND NITROGEN ON IRON AND PYREX AT VERY LOW PRESSURES

by

James Shien-Chung Jen

Dissertation submitted to the Graduate Faculty of the
Virginia Polytechnic Institute and State University
in partial fulfillment of the requirements for the degree of
DOCTOR OF PHILOSOPHY
in
Chemistry

APPROVED:

Dr. J. P. Wightman, Chairman

Dr. J. G. Dillard

Dr. P. E. Field

Dr. J. G. Mason

Dr. T. C. Ward

August, 1973

Blacksburg, Virginia

TO MY PARENTS

ACKNOWLEDGMENT

The author wishes to express his sincerest appreciation to his major advisor, Dr. James P. Wightman, who introduced Surface Chemistry to him and has devoted cooperation, advice, and guidance in the present work as well as in other matters. Deep gratitude and thankfulness are extended to the other members of his advisory committee: Dr. John G. Dillard, Dr. Paul E. Field, Dr. John G. Mason, and Dr. Thomas C. Ward. The author is obliged to

of NASA, Langley Research Center, for his many helpful and invaluable discussions, and for his assistance in constructing the work function measurement apparatus.

The author would like to express his appreciation to

of the Division of Forestry and Wildlife Resource of VPI & SU for his help in taking SEM photomicrograps. He would also like to express his appreciation to of Nuclear Engineering Department of VPI & SU for his help in making Neutron Activation Analysis. Special thankfulness is extended to the Physics Department and the Electrical Engineering Department of VPI & SU, and the NASA, Langley Research Center for their kindness and generosity in loaning the necessary electronic equipment.

He wishes to express his thankfulness to for proofreading the manuscript and to for typing this manuscript.

Last but not least, the author wishes to convey his deepest gratitude to his family and friends in supporting him spiritually throughout his work with their love, kindness, and endless encouragement.

TABLE OF CONTENTS

LIST OF TABLES

LIST OF FIGURES

INTRODUCTION

The study of adsorption of gases on solid surfaces is important for the development of adsorption theories, for the understanding of solid surface properties, and for practical applications. Adsorption studies under ultrahigh vacuum conditions provide information on the interaction between the gas (adsorbate) and the solid (adsorbent) without serious interference from successive adsorbed layers. The solid sample also has less surface contamination under such conditions.

The objective of the present work was to study physical adsorption (chemisorption), of several gas/solid systems at very low pressures. The gases used were Nitrogen, Argon, and Krypton and the solids used were Pyrex and iron. Troy[1] previously studied the adsorption of these same gases on stainless steel. Since stainless steel consists primarily of iron, nickel and chromium, it is of interest to study each of the constituents separately. In addition, Pyrex, and iron alloys are commonly used materials in the construction of ion gauges, vacuum systems, and mass spectrometers.

In this study, the Dubinin-Radushkevich-Polanyi (D-R-P) theory has been used for experimental data analysis.[2-8] However, anomalies in (D-R) plots have been reported.[9-12] Several suggestions have been proposed from thermodynamic as well as experimental points of view to account for the anomalies. It was also the purpose of this work to undertake detailed studies of these anomalies.

Adsorption was investigated in the temperature range 77.4 - 90.2°K, and in the pressure range 10^{-9} - 10^{-5} torr. Surface work function measurements and water contact angle measurements on Pyrex and iron surfaces were added to the above investigations as auxiliary information.

I. THEORY AND LITERATURE REVIEW

A. Gas Adsorption on Solids

The study of the gas/solid interface was the earliest developed branch of surface chemistry, and a tremendous amount of work has been done in this area. However, due to the lack of high vacuum capability in the past, the most of the work was done in the pressure range where multilayer adsorption occurred. Today, with recent developments in high vacuum techniques, it is possible to obtain pressures as low as 10^{-15} torr. General reviews on the gas/solid interface can be found in the books by Young and Crowell,[13] Ross and Oliver,[14] Flood,[15] Adamson,[16] and Somorjai.[17] Hobson[18] has reviewed works within the range from 10^{-4} to 10^{-16} torr. Thus, no attempt is made here to review general works on high vacuum adsorption. The following sections will contain references only to adsorption studies on Pyrex and iron.

1. Pyrex as an Adsorbent

Hobson[19] investigated the adsorption of helium on Pyrex at 4.2°K by using a static ultrahigh vacuum technique, and determined the pressure corresponding to monolayer completion and the helium monolayer capacity. Later, Hobson[20] studied the

adsorption of nitrogen on Pyrex by the same technique at 77.4°K. In this later paper, he was the first to use the Dubinin-Radushkevich theory to interpret this type of data but did not include a detailed discussion of the theory. In 1963, Hobson and Armstrong[2] measured nitrogen and argon adsorption on Pyrex at temperatures from 63 to 90°K for argon and from 63 to 77°K for nitrogen. They found that their experimental data closely followed the equations

$$\Theta = N/N_m = \exp(-B\varepsilon^2) \quad (1)$$

and

$$\varepsilon = RT \ln(P_o/P) \quad (2)$$

where

Θ = surface coverage

N = number of molecules (or atoms) adsorbed per unit area of adsorbent

B, N_m = characteristic parameters

R = gas constant

P = equilibrium pressure of adsorbate

P_o = saturated vapor pressure of adsorbate at T

T = adsorption temperature.

The above equations were first used by Dubinin and Radushkevich[21] to describe the adsorption of organic vapors on porous solids. Equation (2) comes from Polanyi's potential theory.[22,23] Equation (1) is a surface potential distribution function and for this case it is a Gaussian form. In equation (2), ε can be interpreted

thermodynamically as the free energy change of adsorption. The free energy change represents the differential molar work of adsorption done on the adsorbate due to the force field of the solid surface potential. The standard state is taken as the normal liquid in equilibrium with its saturated vapor at temperature T. The gas was assumed to be adsorbed as a liquid-like film.

In the application of this theory it has been generally assumed that all the adsorption sites with energy E equal to or greater than a certain characteristic energy, ε, were occupied by the absorbate and that those sites with less energy did not contribute significantly; that is,

$$E \geq \varepsilon \tag{3}$$

The normalized energy distribution function was recognized as

$$f(E) = \left(2E/E_m^2 \right) \exp-(E/Em)^2, \tag{4}$$

where E_m was interpreted as the mean adsorption energy of the system by Hobson and Armstrong.[2]

Integrating Equation (4) from ε to ∞ as indicated in Equation (3) leads to

$$\theta = \int_{\varepsilon}^{\infty} (2E/E_m^2) \exp -(E/E_m)^2 \, dE$$

$$= \exp -(E/E_m)^2. \qquad (5)$$

Equation (5) is equivalent to Equation (1) with

$$B = 1/E_m^2, \qquad (6)$$

and it is experimentally found that B is primarily dependent on the adsorbate. Mirsa[24] and Cerofolini[25] later theoretically interpreted E_m as the heat of adsorption for the most prevalent sites rather the mean adsorption energy.

It is somewhat misleading that mobson and Armstrong[2] considered the parameter E_m as the mean adsorption energy. From Equation (4), the mean energy can be obtained as,

$$\bar{E} = \int_{\varepsilon}^{\infty} Ef(E) \, dE$$

$$= \int_{\varepsilon}^{\infty} (2E^2/E_m^2) \exp -(E/E_m)^2 \, dE$$

$$= (\Pi/4)^{\frac{1}{2}} B^{-\frac{1}{2}} - \int_0^{\varepsilon} Ef(E)\ dE. \qquad (7)$$

The second term is quite small and can be evaluated numerically. It is always a positive term, and is also a function of ε. In this thesis, however the second term was not evaluated, and the quantity $(\Pi/4)^{\frac{1}{2}} B^{-\frac{1}{2}}$ was used as a limiting (maximum) value of the mean adsorption energy for comparison purposes.

The other characteristic parameters in Equation (1) is N_m. Kaganer [26] described the constant N_m as a limiting value of the number of molecules (or atoms) adsorbed at monolayer coverage.

The Polanyi potential theory assumes that the adsorption potential energy of the adsorbent is independent of temperature; that is,

$$d\ \varepsilon/dT = 0 \qquad (8)$$

and hence

$$d\Theta/dT = 0. \qquad (9)$$

This means that the characteristic curve, representing the potential energy distribution, i.e., $\varepsilon = f(\Theta)$, is the same at all temperatures, as is also true for the function $\varepsilon^2 = f'(\Theta)$.

From equation (1), a plot of ln N versus ε^2 should give

a straight line with an ordinate intercept of ln N_m and a slope of -B. From Equation (8) all the lines obtained from plotting adsorption data taken at different temperatures should coincide.

Hobson and Armstrong[2] indeed not only found the temperature-independent property of the Polanyi theory but also confirmed Kaganer's interpretation of N_m as the number of molecules absorbed at monolayer coverage. These authors also correlated the constant B as the inverse of the square root of the mean absorption energy.

Ricca and Medana[27] studied the adsorption of nitrogen and methane on Pyrex by a dynamic technique. Ricca, Medana and Bellarde[3] measured the adsorption of argon, krypton and xenon on Pyrex and later [4] the adsorption of carbon monoxide on Pyrex. Adsorption on Pyrex has also been studied by Endow and Pasternak,[9] Baker and Fox,[28] Tuzi and Saito, [5] and Outlaw.[29] All these investigators reported that their results obeyed the Dubinin-Radushkevich-Polanyi (D-R-P) theory.

Haul and Gottwald[30] studied the adsorption of Ar, Kr, and Xe on Pyrex. Their Adsorption data for argon were taken in the temperature range from 83 to 100°K, and fit the D-R-P theory. However the D-R line obtained for the argon/Pyrex system was parallel but considerably higher than the line from Hobson and Armstrong's data[12] in the temperature range from 63 to 77°. No explanation was given for this discrepancy of the temperature-independent property of the theory.

Jen and Wightman[12] reported their studies of argon adsorbed on Pyrex at four different temperatures (77.0, 81.4, 87.5 and 90.0°K), and found two parallel D-R lines. One line represented data at 77.0 and 81.4°K and the other line represented data at 87.5 and 90.0°K. The existence of two lines was attributed to phase transitions of argon upon adsorption on the Pyrex surface. Parenthetically, this result was noted similar to a combination of the works of Hobson and Armstrong,[2] and Haul and Gottwald.[30]

2. Iron as an Adsorbent

Studies of chemically adsorbed gases have been generally done with metals such as Ni, Pt, Au, Ag, W. Fe, Zn, Ti and metal oxides.[31] The frequent study of these metals and oxides is due to their great catalytic properties. Few studies have been reported in the area of physisorption of gases on iron surfaces. Since iron is the main component of stainless steel, it is of interest to study pure iron itself.

Scholten, Zwietering, Kovalinka and de Boer[32] measured the rate of adsorption of nitrogen on an iron catalyst by means of a vacuum balance. In this case, chemisorption of nitrogen was indicated.

Granville and Hall[33] studied the adsorption of krypton on iron films at 76°K. Type II isotherms were obtained for the system. Monolayer volumes, determined by the Kaganer method, were compared with the BET values. The ratio of the former to the latter varied between 0.55 and 1.1 for different iron film preparation.

Hall and Hope[34] investigated the adsorption of argon, krypton, nitrogen and hydrogen on an iron film and on catalyst sponges of iron at temperatures between 76 and 154°K. At low temperatures, the argon, krypton and nitrogen isotherms were type II. The isotherm of hydrogen adsorbed on iron was close to the Henry Law's Limit. Isosteric heats of adsorption indicated that all gases were physisorbed.

The chemisorption of nitrogen and hydrogen on iron surfaces has been reported elsewhere.[31] The question of whether nitrogen is physisorbed or chemisorbed on iron is still not resolved.

3. Other Important Works

Schram[10] investigated the adsorption of argon on nickel between 78 and 120°K, and he did not obtain the temperature invariant property of the potential theory as predicted by Equations (1) & (2). Later Schram theoretically showed that the parameter B is indeed slightly dependent on temperature.[35] Endow and Pasternak[9] also found that their results for the adsorption of krypton and xenon on Pyrex and on molybdenum film did not follow the temperature independent property of the potential theory. These authors attributed the discrepancy to temperature gradients at the cooled adsorption surface, and hence to an uncertainty in the temperature of the adsorbent. Troy and Wightman[11] reported the results for the adsorption of argon, krypton, methane

and nitrogen on 304 stainless steel. This work was of particular relevance to the present work since basically the same vacuum system, but with different adsorbents, was used in both studies. From their results they also did not find the temperature invariant property which the theory predicts.

4. Modification of the Theory

As noted above some attention has been given to the anomalies of lines in the D-R plots. Aside from possible experimental errors, Bering and Serpinskii[36] argued the applicability of the D-R-P theory from a thermodynamic point of view. These authors concluded that the above theory is valid only within the adsorption range where the entropy of adsorptions $\Delta S_{ads} < 0$. This is a necessary but not sufficient condition. Dovaston, McEneney and Weedon[37] supported the above argument theoretically, and experimentally found an application limit of $P/P_o > 10^{-3}$ for the adsorption of carbon dioxide on microporous carbons. Maggs[38] also showed numerically why the temperature invariant property of the D-R-P theory should be followed. However, all these authors considered only the high surface coverage region, that is, when multilayer adsorption occurs.

It is certainly unrealistic to consider the adsorbed phase as a normal liquid-like one in the very low surface coverage region of the present study. Since there are not many molecules (or atoms)

adsorbed, e.g., $\theta = 10^{-6} - 10^{-3}$. This is particularly true if the adsorption is localized. Whether adsorption is localized (immobile) or mobile, there is always a positive contribution to the total entropy change of adsorption from the configurational entropy ($\overline{S}_{config}$) except on an extremely heterogeneous surface. For example, for localized Langmuir adsorption,

$$\overline{S}_{config} = -R \ln \theta/1-\theta, \tag{10}$$

and for mobile two dimensional ideal gas adsorption,

$$\overline{S}_{config} = -R \ln \theta - R. \tag{11}$$

Thus for both types of adsorption, small values of θ correspond to positive values of $\overline{S}_{config}$.

Then the important question arises as to the proper choice of the standard state of the adsorbed phase. Unfortunately, not very much is known about the nature of the adsorbed phase at very low surface coverages.

In the early development of the Polanyi theory, Berenyi[13] defined three adsorption cases, which are summarized in Table 1. The variation of the adsorbed phase density for these cases versus the potential field is shown in Figure 1. It is clear that in

TABLE I. THREE ADSORPTION CASES

Case	Adsorption Temp*	State of Adsorbed Phase
I	Well below T_c	Liquid
II	Just below T_c	Liquid and Compressed Gas
III	Above T_c	Compressed Gas

* T_c is the critical temperature of the adsorbate.

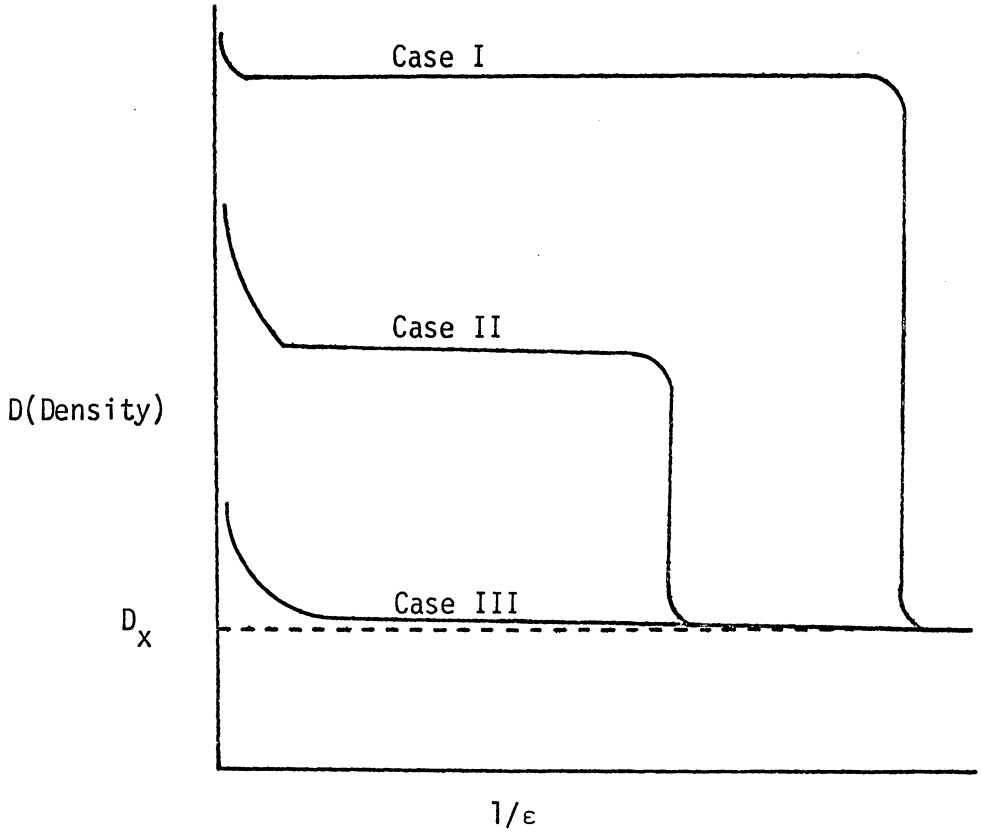

Figure 1. Variation of the density within the adsorbed phase according to the potential theory. (Reference 22). Where D_X is equal to the density of the gas and $1/\varepsilon$ is the inverse of surface potential (adsorption volume was used in the original graph).

Case III, the density of the adsorbed phase is far smaller than that of the liquid. This situation is exactly the same as adsorption at the very low surface coverages in the present work even though the adsorption temperature is below the critical point.

For Case III, Berenyi[39,40] modified Equation (2) and derived a new form as,

$$\varepsilon = RT \ln(0.14\ T/bP) \tag{12}$$

where b is the van der Waals' constant. Subsequently, Nikolaev and Dubinin,[41] based on Equation (12), reported the empirical expression as,

$$\varepsilon = RT \ln (\tau^2 P_c/P) \tag{13}$$

where τ = the reduced (corresponding state) temperature, i.e., $\tau = T/T_c$

P_c = the critical pressure of adsorbate.

Both Equations (12) and (13) were proposed for multilayer adsorption at temperatures higher than the critical temperature, and were shown to be experimentally satisfactory.[42]

It is proposed in this thesis that Equation (13) may be used for low surface coverage adsorption, even at adsorption temperatures lower than T_c. The rationale for using this equation is that we now change the standard state of the adsorbed phase from the normal

liquid-like phase to a non-specific adsorbed phase. This less dense adsorbed phase can be characterized by the empirical equation

$$p^o = \tau^2 P_c = (T/T_c)^2 P_c. \qquad (14)$$

So far, the use of Equation (13) for adsorption has been limited to high pressure adsorption. The extension of Equation (13) to low pressure adsorption data is shown in the Results and Discussion chapter.

5. Isoteric Heat of Adsorption

From the definition of isosteric heat of adsorption (14) we have that

$$(\partial \ln P/\partial T)_\Theta = q_{st}/RT^2, \qquad (15)$$

where q_{st} = the isoteric heat

R = the gas constant.

A plot of ln P against 1/T gives a straight line with the slope of $-q_{st}/R$.

B. Work Function

1. Theory

The measurement of the work function has been used for many years in monitoring the condition of surfaces. The relative change in the work function gives information on changes in surface state. For example, when a gas molecule is adsorbed on a metal surface, the outer shell electrons of the adsorbate are disturbed. In the case of physisorption, electrons are polarized by the metal surface. Charge is transferred to the metal in the case of chemisorption. This perturbation of electron distribution can be observed through the work function change. The adsorbed molecule represents generally a negative charge center that tends to inhibit the electrons' escape, thus increasing the work function.

Although the work function of a surface can be determined directly, it is the work function change of the surface state which is of interest. The greater the surface state change, the larger the work function change.

There have been several techniques[43,44] commonly used to measure work function. General reviews on different techniques were given by Riviere,[45] Eberhagen,[46] Culver and Tompkins,[47] and Sachlter.[48]

The retarding field diode technique [49-51] was adopted in this work. Recently, Knapp[52] has published an excellent review specifically on the theory and techniques of the diode method. In this technique, a hot filament emits electrons. At low current density these electrons build up a space charge at the surface and produce an electrostatic barrier to prevent electrons from flowing to the anode (test sample). This energy barrier is higher than the surface barrier, that is, the retarding potential region. The current passing through the anode is controlled by an applied potential. The electron flux is then plotted as a function of the applied potential between the anode and cathode, a Richardson plot. The average anode work function is obtained from such a plot. The shift in the Richardson plot with changes in surface condition determine the work function change.

A simple derivation of the relevant equations is shown as follows. Basically, the electron flux which is emitted by the hot filament (cathode) and impinges on the adsorption vessel (anode) is dependent on the cathode work function (ϕ_c) and the cathode temperature only. The fraction of electrons received by the anode depends only on the electron energy and the work function of the anode. Therefore, if the temperature of the cathode (T) is well controlled, the receiving electron flux is dependent only on the work function difference and the voltage difference between the cathode and the anode.

In the retarding field region, the energy barrier is such

that the anode Fermi surface is higher than that of the cathode as shown in Figure 2. The applied voltage between the cathode and anode (V_a) then determines the barrier height and the fraction of the electrons reaching the anode. The anode current is given by[29]

$$I = A\,T^2 \exp\{-(\phi_a - V_a)/kT\} \qquad (16)$$

where I = current

ϕ_a = anode work function

A = constant

k = Boltzmann's constant

The current through the diode is,

$$V_b - V_a = IR = V_R$$

where V_b = applied voltage (see Figure 9)

R = resistance (see Figure 9)

V_R = voltage drop through resistance.

Taking the logarithm of Equations (16) and (17), and differentiating gives

$$dI/I = (d\phi_a/kT) + (-dV_a kT)$$

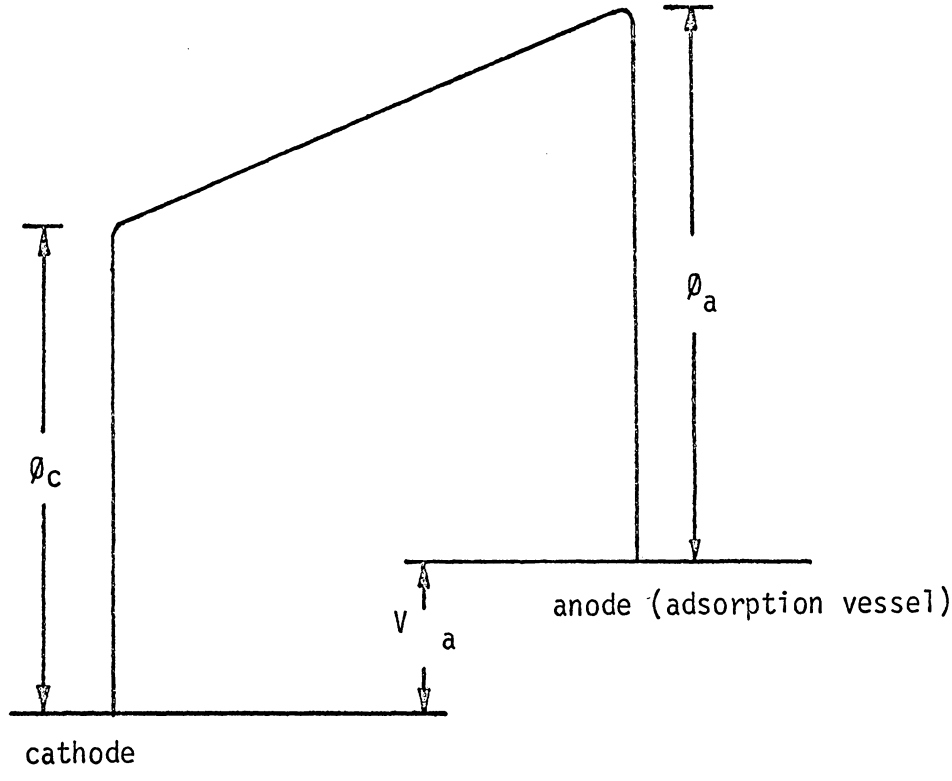

Figure 2. Electron potential energies in the retarding field.

and $$dI/I = \{R/(V_b - V_a)\}\ (-dV_a/R).$$

Combining the above two equations gives

$$(-d\phi_a/kT) + (dV_a/kT) = -dv_a/(V_b - V_a)$$

so that

$$d\phi_a/dV_a = 1 + kT/(V_b - V_a)$$

and if

$$kT/(V_b - V_a) >> 1$$

then

$$\Delta\phi_a \simeq \Delta V_a \qquad (18)$$

thus the difference between the anode and cathode voltages gives the change of the anode work function.

The relationship between surface coverage (θ) and work function (ϕ) was given as,[44]

$$\phi = \phi_o \pm 4\pi N\mu\theta \qquad (19)$$

where

ϕ_o = work function of clean surface

N = adsorbed number of unit area

μ = dipole moment for the system

This theory predicts a linear relationship at low coverages (at $\Theta < 0.5$), but a nonlinear relation at high coverages.

A typical retarding field plot is shown in Figure 3. Ideally, in the retarding field region, the logarithm of the current rises linearly as the applied potential increases, and then levels off when it reaches saturation. However, in the actual case, due to the applied electric field, the current continuously rises.

Firgure 4 demonstrates the related work function change in the retarding field region due to different emission currents (I_1 and I_2).

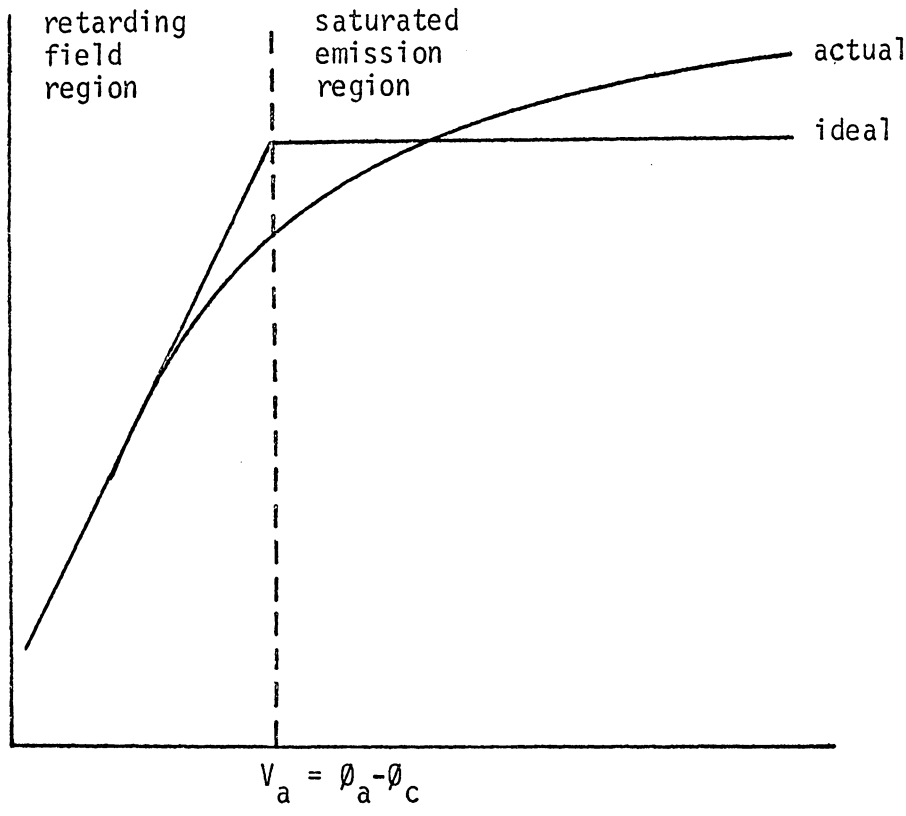

Figure 3. Retarding field characteristic curve.

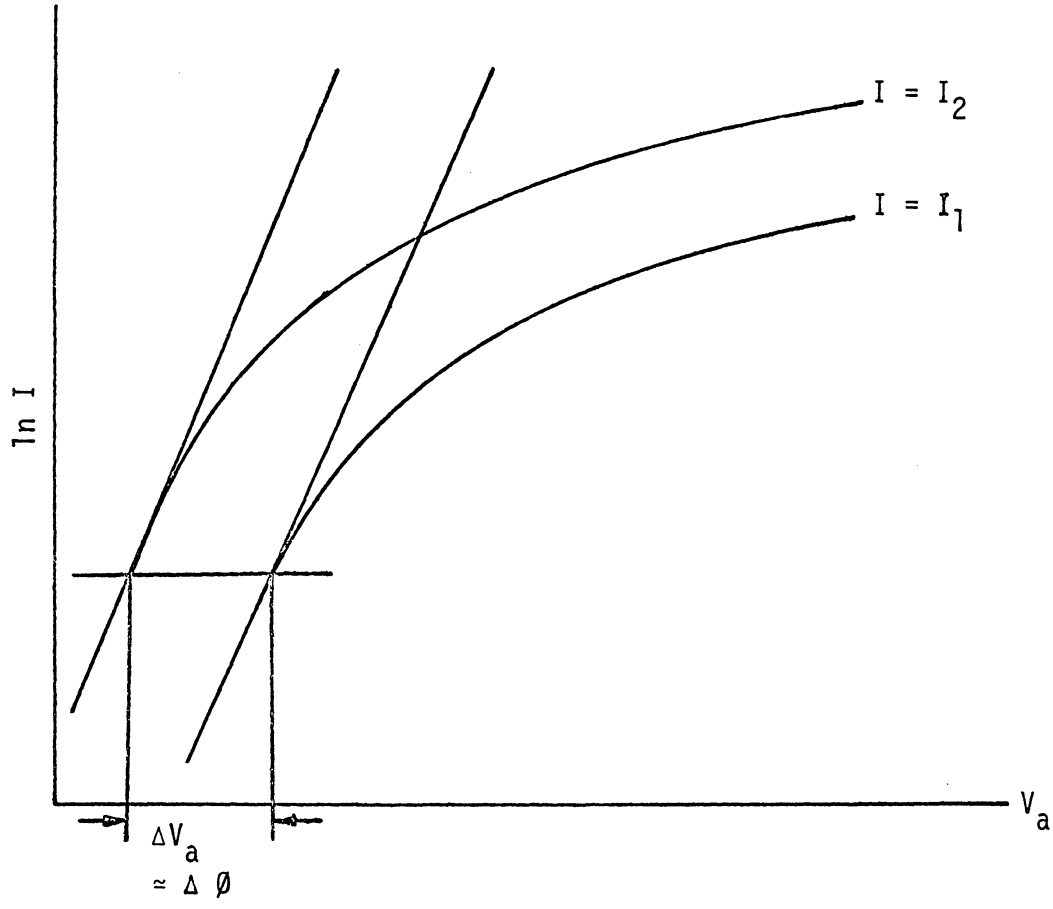

Figure 4. Work function change in the retarding field

2. Iron

Work function measurements of gases adsorbed on iron surfaces have been reported. However, most of these were chemisorption studies, and physisorption studies have been reported only rarely.

Klemperer and Snaith[53] studied the changes of work function of xenon physically adsorbed on iron, copper, and sodium at different metal annealing temperatures by using the diode technique. They found that the surface roughness was an important factor which caused the work function to decrease as the surface roughness decreased.

C. Contact Angle

Contact angles were measured in this thesis since such measurements are sensitive to solid surface contamination and to surface roughness. The theory of contact angles has been well developed elsewhere[16,54] and several comprehensive reviews exist.[55,56]

There has been a fair amount of work on the effect of contamination on contact angles on metal and glass surfaces,[57,60] but surprisingly, very few references could be found for studies of contact angles of water on bare glass and iron surfaces.

Tamai, Makuuchi and Suzuki[61] introduced the technique of interfacial contact angle measurements on metal surfaces. Advancing contact angle (θ), for the system, n-octane-water-iron, were found in the range of 81.0 to 84.0°. Bernett and Zisman[62] investigated the contact angles of a series of hydrocarbons on metals including iron and iron oxide under different controlled relative humidity enrivonments. The physisorbed thin film of water was found to be responsible for decreasing the critical surface tension. Elliott and Riddford[63,64] examined the forced spreading of water on siliconed glass surfaces. The static advancing contact angle was reported to be 105°, and the dynamic contact angles were reported. The advancing and receding contact angles were found dependent on the interfacial velocity. Tamai and Aratami[65] studied contact angles in the mercury/silica glass system and correlated their results to the surface roughness through Wenzel's relation.[66] Barnal[67] attempted to calculate the contact angle of water on glass surfaces by measuring the volume and the height of the drop. However, his results were non-reproducible.

Jen[68] measured the contact angle of water on quartz cleaned separately with detergent, chromic acid, cleaning solution and hydrochloric acid, and found an average value of 31 ± 8° at room temperature. He also found an average water contact angle of 35 ± 15° on quartz washed with Xerox fluid (isopropyl alcohol). Also, he found an average water contact angle of 6 ± 2° for a

quartz sample heated to 300°C in air for 2 hours. Koranyi and Acs[69] found that water contact angles on lime silicate glass treated with various organic solvents, hydrochloric acid and distilled water ranged from 2 to 65°. A value of 4° was obtained by heating the glass to 300°C for 2 hours. The elapsed time at ambient temperature after heating was found to be critical. The contact angle increased from 4 to 23° after an elapsed time of 8 hours.

The above three works are of particular interest, since zero water contact angles on quartz and on glass are generally assumed in many areas of study. Evidently, a wide range of contact angles of water on glass have been reported and even after many different treatments, the angle is not reduced to zero. Further, the water contact angle on quartz and glass seems extremely sensitive to the history of the solid sample.

II. EXPERIMENTAL

A. Adsorption Isothem Measurements

In general, there are two types of experimental tecyniques used in low pressure adsorption studies, namely, the dynamic and the static. The dynamic technique has been quite commonly used for many years.[70] This technique involves passing gas at a constant rate into the test chamber, which is connected to the pumping system. The pressure inside the system is monitored continuously. At the onset of adsorption, the pressure decreases and then returns to its original value after adsorption is complete. An integration of the pressure change over the time period, via a molecular balance equation, gives the amount of gas adsorbed. The main disadvantages of this method are (1) very precise control of gas flow rate is required, (2) long equilibration times are necessary at low pressures, and (3) low sensitivity to adsorption at very low surface coverages is observed. In the static technique, the test chamger is isolated from the pumping system while making the adsorption measurement. The pressure change of the constant volume system during adsorption is directly related to the amount of gas adsorbed. The major disadvantage of the static technique is the ion gauge pumping effect. In the present study, the experimental work was carried out via the static technique and a detailed description is presented in the following sections.

1. Apparatus and Procedure

A schematic diagram of the apparatus is shown in Figure 5. The test vessel was connected to an ionization pump (I.P.) (Varian, Model 912-6000) and a titanium sublimation pump (S.P.)(Varian, Model 916-0014) through a Granville-Phillips auroseal ultrahigh vacuum valve (G.P.) (Granville-Phillips, Series 267). The capacities of these pumps were 50 l. sec^{-1} and 350 l. sec^{-1}, respectively. The idea behind using these pumps was to minimize contamination of the adsorption surfaces. Prior to adsorption measurements, all the valves except the G.P. valve were closed. The pressure inside the vacuum system was kept at about 10^{-11} torr and was monitored by a Bayard-Alpert type ionization gauge (I.G.) (Varian, Model 971-5008). The ion gauge was connected to an ionization gauge control unit (I.G.C.). (Granville-Phillips, Model 02). The pressure as an analog signal was read directly from the front panel in terms of torr, and the output was recorded by using a Moseley strip chart recorder (R) (Hewlet-Packard, Model 680). Operating conditions of the ion gauge will be discussed in a later section. Prior to each series of adsorption runs, the gauge was degassed for approximately 15 to 20 minutes by electron bombardment at 60 watts. The gauge was then cooled for about two hours to allow the system reach a steady-state pressure. While making a run, the gas inlet was first evacuated by a Vac-Sorb pump (V.P.) (Varian, Model 941-6001). The pressure in

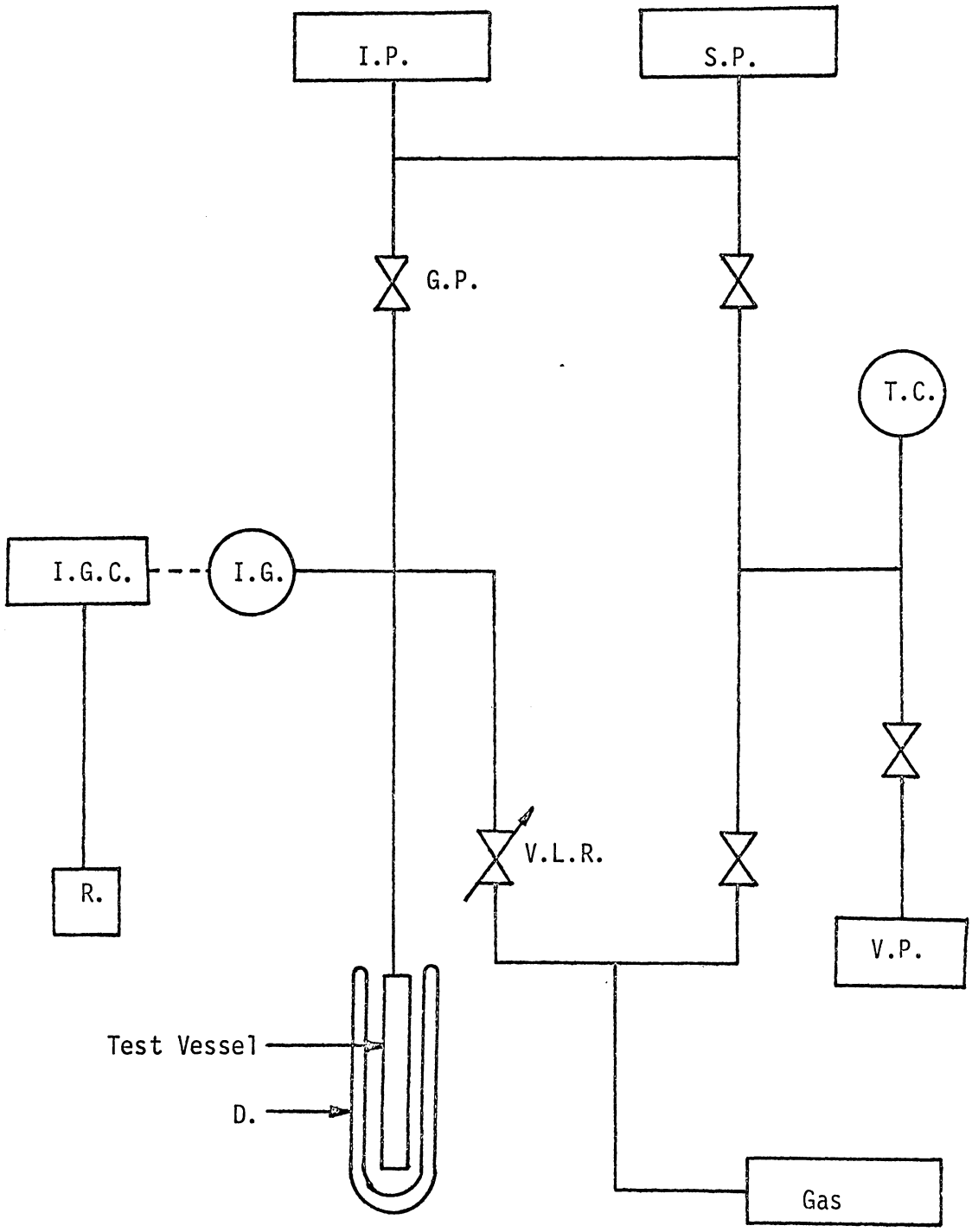

Figure 5. A schematic diagram of ultrahigh vacuum adsorption system.

the inlet line was monitored by a thermocouple gauge (T.C.) (Hasting Type DV-6M). After the inlet line was evacuated, the G.P. valve was closed to isolate the system from the pumps. The test gas then was introduced into the main system through a variable leak rate valve (V.L.R) (Varian, Model 951-5100) until a desired pressure was reached. Again a sufficient period of time elapsed to let the system reach a steady-state. This time was typically ranged from 10 to 30 minutes but different from gas to gas. A dewar flask (D). filled with a specific cryogenic fluid was then raised up to immerse the test vessel to a desired level. Again, a sufficient period of time elapsed to allow the system to reach a steady-state pressure. The G.P. valve was then opened to evacuate the gas, and the system was ready for the next run. The solid sample was actually included as a part of the ultrahigh vacuum system. This eliminated the difficulty of cooling the adsorbent when the pressure was so low that gaseous thermal conduction approaches zero which is a serious problem with finely divided adsorbents.[71]

A typical pressure versus time trace obtained during a run is shown in Figure 6. The positive slope was due to the ion gauge pumping effect which is discussed in the next section. The line AB is an extended line of the horizontal portion of the pressure versus time trace, which represents the rapid pressure change of the system due to the adsorption after the sample vessel was immersed into the cryogenic fluid. Pressures P_1 and P_2 are described in the next section.

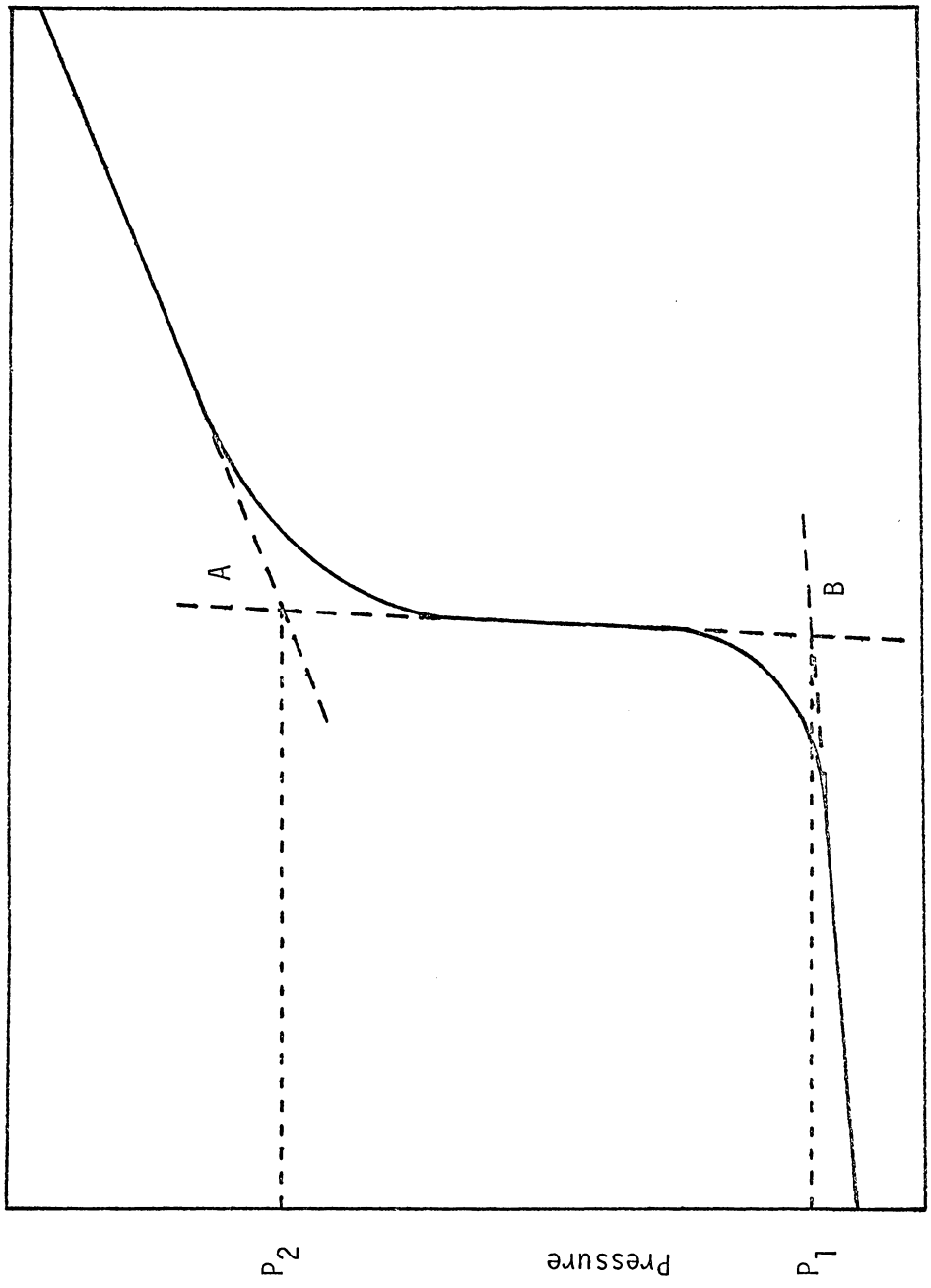

Figure 6. A typical pressure-time trace plot.

2. Ionization Gauge Operation

It is well-known that an ionization gauge acts as a pump in a vacuum system and this pumping effect is even more significant at low pressure. There have been different methods suggested for minimizing this effect.[1,2] One of the ways is to lower the filament current as was done in this work. Following suggestions of previous work,[1] the emission current was reduced to 40μA as indicated by the positive slopes in Figure 6. This problem was minimized by waiting for a sufficient period of time until no further slope change occurred in both the pre- and post-adsorption portions of the pressure-time trace. Pressures P_1 and P_2 in Figure 6 were obtained by extrapolation of both straight ends to the line AB. Long equilibration time studies were also carried out and it was found that even after three hours there was no significant change in slopes as compared to the shorter equilibration time traces. These studies gave a good indication that adsorption on the solid surface approached an equilibrium state. The ion gauge was not calibrated and the "nitrogen equivalent pressure" is used throughout this study.

3. Cryogenic Fluid

The temperatures used for adsorption studies in most of the gas/solid systems were 77.4 and 90.2°K, achieved by means of liquid nitrogen and liquid oxygen. For the argon/Pyrex system, two additional temperatures used were 81.8 and 88.1°K. These two temperatures were obtained by mixing appropriate amounts of liquid nitrogen and liquid oxygen in a dewar. Helium was bubbled through to assure proper mixing. The temperature of this "liquid air" bath was monitored by an oxygen vapor pressure thermometer.

4. Gases

The following gases used in this work were all obtained from the Matheson Co. as research grade gases with the indicated purity: nitrogen (99.999%), argon (99.995%) and krypton (99.995%). Mass spectroscopic analysis showed that the major impurity in nitrogen was carbon dioxide, in argon was carbon dioxide, and in krypton was argon.

5. Pyrex Finger

The pyrex finger shown schematically in Figure 7 was made of Corning 7740 glass and fabricated in the glass shop of the Chemistry Department at Virginia Polytechnic Institute and State

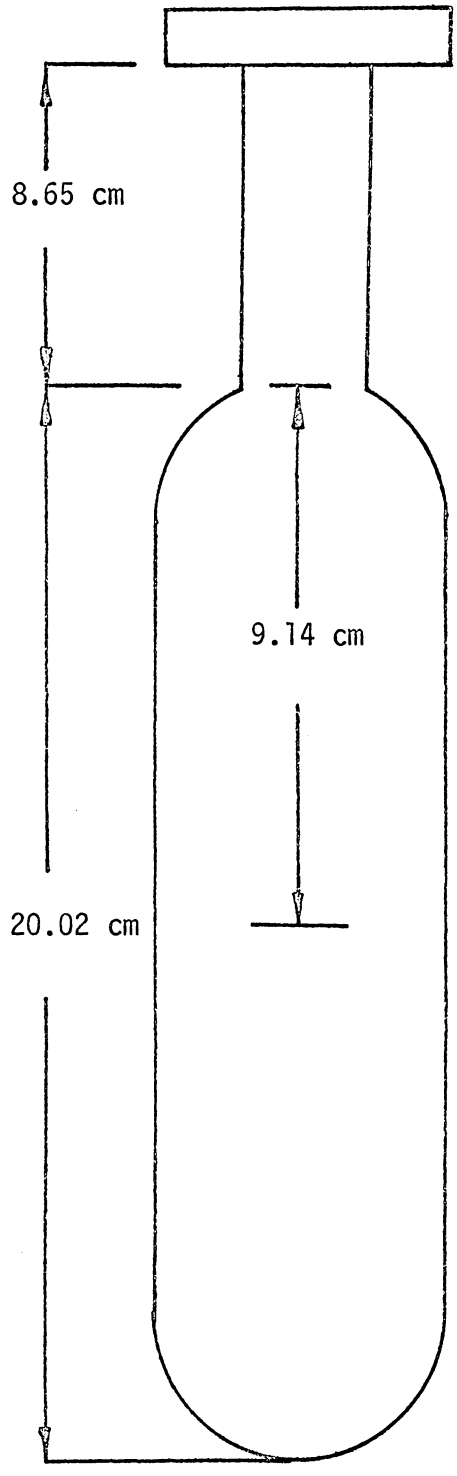

I.D. = 1.64 cm

level I

Level	Area (cm^2)	Volume(cm^3)
I	237	213
II	128	115

level II

I.D. = 3.80 cm.

Figure 7. The geometry of the Pyrex finger.

University. The Pyrex finger was first fire polished and then annealed in an oven up to 300°C for 12 hours. The finger was rinsed with ethylene dichloride prior to mounting it on the high vacuum system. No further surface treatment of the finger was given. After mounting the finger, the whole system except the pumps was baked-out up to 150°C for 72 hours in order to expel adsorbed water and any low vapor pressure organic contamination.

As indicated in Figure 7, there were two levels marked on the Pyrex finger for the purpose of investigating any possible non-isothermal hot flux phenomenon. A heating tape was wrapped around the finger just above the particular level. The temperature was maintained at 0°C and was monitored by a chromel-alumel thermocouple and read out on a potentiometer (Leeds and Northrup 7754, Type K-4).

The following elemental composition of the Pyrex finger was obtained by neutron activation analysis (NAA) at the Virginia Polytechnic Institute and State University:

Element	Concentration (ppm)
Al	352
Br	21
Cl	557
Cu	171
K	703
Na	1222
Ru	67

Sb	49
Zn	176

However, these results show only the composition of the bulk. The surface was analyzed by using Electron Spectroscopy for Chemical Analysis (ESCA) and Scanning Electron Microscopy (SEM). The results of these analyses are discussed in the Results and Discussion chapter.

6. Iron Vessel

The 99.99% pure iron vessel was obtained from the Materials Research Corporation (MRC). It was cast and machined to the dimensions shown in Figure 8. An absorption spectrographic analysis made by MRC showed the following major bulk impurities:

Elements	Concentration (ppm)
C	30
O	78
Gr	10
Co	10
Cu	40
Mn	20
Ni	10
P	20

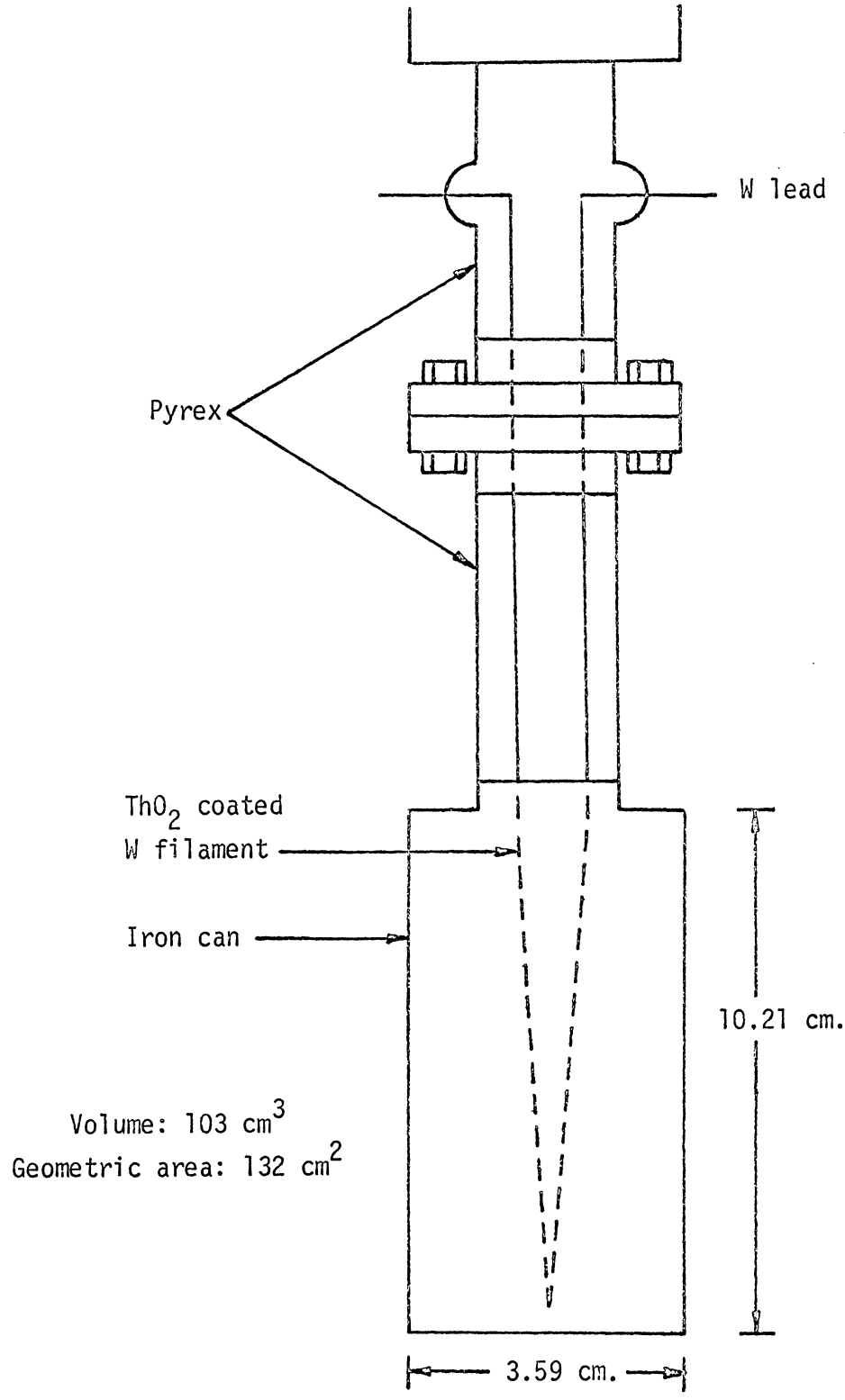

Figure 8. The geometry and work function filament arrangement of the iron vessel.

Si	35
S	30

The surface treatment of this iron vessel was the same as that for the Pyrex finger. During each run a heating tape was placed at the neck of the iron vessel in order to maintain a defined adsorption surface.

ESCA and SEM Analyses were also made on iron vessel and the results are discussed in the Results and Discussion chapter.

7. Diversey Cleaning Process

After isotherms were measured on the iron vessel described above, the vessel was further treated with the Diversey process. This is one of the common commercial surface cleaning processes that was developed by the Diversey Company, California, U.S.A. The process contains four major steps, namely, (1) degreaser- a noncaustic, alkaline cleaner to remove the surface organic contamination, (2) oxidizer - a highly alkaline material containing caustic soda and an oxidant which sets up the surface oxides for easier removal, (3) oxide remover- a mixture of acids to remove the surface oxides, and (4) etchant - a concentrated acid for etching. Each step was immediately followed by a de-ionized distilled water rinse. The purpose of this particular treatment was to investigate

the effect of chemical cleaning by a commercial process on the adsorption isotherms. The effect of this process on the iron surface was examined via ESCA and SEM, and the results of these analyses are given in the Results and Discussion chapter.

B. Work Function Measurements

A schematic diagram of the work function circuitry is shown in Figure 9. The arrangement of the filament in the iron adsorption vessel is shown in Figure 8. The cathode filament was made of 0.005 in. diameter tungsten wire and coated with thoria.

The filament current was supplied from a power supply (Eastern Scientific Instrument Corp., Model RVC 36-15), and was read via a current-meter (Weston Electrical, Model 430). The standard dc voltage came from an Ambitrol V-1 Transistorized Power Supply (Power Design Inc.), and read out through a digital voltmeter (United Systems Corp.). The differential voltmeter, V_a, was a Potential Electrometer (Keithley 630).

The filament current and standard dc voltage supply were preset in order to keep within the retarding field region. For example, with the nitrogen/iron system, the filament current was set at 1.99 A, and the standard dc power supply was set at 4.00 V. Prior to and at the end of each adsorption run, work function changes were calculated, i.e., the readings of V_a were read on the differential voltmeter.

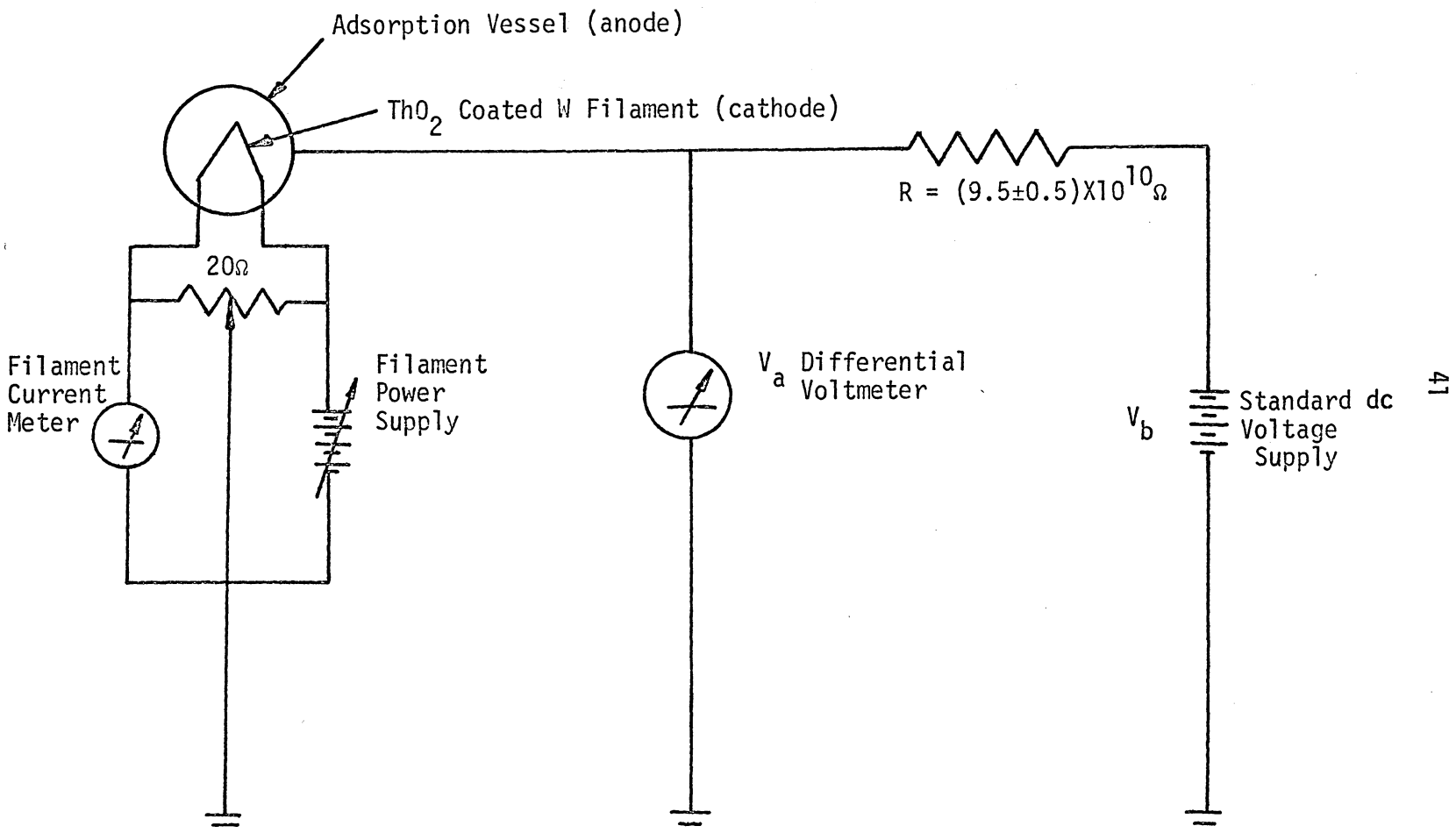

Figure 9. Schematic diagram of work function circuitry.

C. Contact Angle Measurements

Water contact angle measurements on Pyrex and iron were made at room temperature in the laboratory environment. The Pyrex and iron samples were pre-cleaned in the same way as those in the isotherm studies. A special cell was built to measure the water contact angles. A water droplet was placed on the sample surface from a 1 ml. syringe. Each drop had an approximate volume of 0.03 ml. The contact angle was then measured by using a comparator microscope fitted with a goniometer scale (Gaertner Scientific Corp.). The water used in this study was deionized and distilled in a quartz still (Kontes, Model WS-2) and stored in a polyethylene container.

III. DATA ANALYSIS

A. Adsorption Isotherm Measurements

Experimental data obtained from pressure-time traces (see Figure 6) were reduced by a modified ideal gas equation given below in order to evaluate the amount of gas that was adsorbed on the surface.

$$N = (N_o/RA)\ \{(P_1V/T_1) - (P_2V_h/T_1) - (PV_c/T_2)\} \tag{20}$$

where N = number of molecules (or atoms) adsorbed per unit area

N_o = Avogadro's number

R = ideal gas constant

A = geometric sruface area of solid adsorbent

P_1 = steady state pressure prior to adsorption (see Figure 6)

P_2 = equilibrium adsorption pressure (See Figure 6)

P = equilibrium adsorption pressure after thermal transpiration correction

V = total volume of the system

V_c = fraction of V below the cryogenic bath level

$V_h = V - V_c$

T_1 = pre-adsorption temperature (i.e., room temperature)

T_2 = adsorption temperature (i.e., cryogenic temperature).

The first term in the bracket is the total number of molecules (or atoms) of gas initially present in the system. The second and third terms represent the amount of gas remaining in the gas phase at temperatures T_1 and T_2.

B. Thermal Transpiration Effect

Thermal transpiration, also known as thermal effusion, was first discovered by Neumenn,[72] and extensively studied by Reynolds, Maxwell, and many others.[73-75] This phenomenon is the existence of pressure differences produced by temperature differences in the same system at low pressures. It has been demonstrated to be a very important effect in high vacuum adsorption studies.[76-79] It is generally accepted that in free molecular flow, the following square-root relation holds between pressure and temperature:

$$P/P_2 = R_t = (T_1/T_2)^{\frac{1}{2}} \qquad (21)$$

where R_t is the transpiration constant, and the subscripts 1 and 2 refer to the pre-adsorption and adsorption states, respectively.

There are other empirical equations such as the one derived by Liang[80-83] and subsequently modified by Bennett and Tompkins,[84] and the one derived by Weber[85] and modified by Sin.[86] All these formulas were derived for more restricted molecular considerations. Hosever, a comparative study was made for each set of absorbate/adsorbent systems and system geometries in the present work and it was found that Equation (21) was suitable for all cases.

C. Vapor Pressure of Adsorbates

Vapor pressures, P_o, used in Equation (2) for calculating ε were calculated from the following equations:[1]

Argon(solid)	$P_o = 7.59 \times 10^7 \exp(-992/T_2)$
Argon(liquid)	$P_o = 5.31 \times 10^6 \exp(-772/T_2)$
Krypton(solid)	$P_o = 2.39 \times 10^7 \exp(-1258/T_2)$
Krypton(liquid)	$P_o = 2.23 \times 10^7 \exp(-1245/T_2)$
Nitrogen(liquid)	$P_o = 6.96 \times 10^6 \exp(-706/T_2)$

Since the lowest adsorption temperature was that of liquid nitrogen, the vapor pressure of solid nitrogen was not included.

D. Data Reduction

All the Dubinin-Radushkevich(D-R) plots were linearized via a (FOCAL) linear regression program using a PDP8/I computer. The isotherms were fitted using a (FORTRAN IV) polynomial regression program through an IBM 360 computer system. In both cases, the confidence limit of F-test was set equal to 95%.

All isotherm measurements were taken with the background pressure $<10^{-10}$ torr at an emission current of 40 μA. Thus, there was some background gas interference in the low pressure range but this interference was less significant in the higher pressure range. This effect was not corrected for in the results, since the background gas composition was not obtained in the present study.

E. Effect of Work Function Measurement on Adsorption Measurements

Thermionic electrons from the filament struck the adsorbent surface while the work function change was measured during adsorption. The question arises whether this could cause a perturbation of the physically adsorbed molecules. This problem can be analyzed by comparing the incident electron flux to the number of adsorbed molecules. For typical work function measurement conditions, an incident electron flux of $6X10^{8}$ electrons cm^{-2} is calculated in Appendix I.

The perturbation of work function measurements on adsorption measurements was expected to be significant as discussed in the Results and Discussion chapter.

F. Contact Angle Measurements

All the contact angle data were statistically averaged by a standard least squares method as follows.[87]

$$\text{mean} = (m_1 + m_2 + \ldots\ldots\ldots + m_n)/n$$

and

$$\bar{d} = \{(d_1^2 + d_2^2 + \ldots\ldots\ldots + d_n^2)/ (n-1)\}^{\frac{1}{2}}$$

where m_i = the i-th measurement

d_i = deviation from the mean

$\bar{d}$ = standard deviation

n = total number of measurements

IV. RESULTS AND DISCUSSION

A. Adsorption Isotherms

1. Pyrex

The D-R plots of nitrogen adsorbed on Pyrex are shown in Figures 10 and 11. The plot in Figure 10 was based on Equations (1) and (2), where P_o was the vapor pressure of liquid nitrogen at the specific adsorption temperature. The Straight, temperature-invariant lines having different intercepts and slopes were obtained in both cases. The N_m and $(\pi/4)^{\frac{1}{2}}(B)^{-\frac{1}{2}}$ values calculated from Figures 10 and 11 were $1.87X10^{14}$ molecules cm^{-2} and 1.64 kcal mol^{-1}, and $4.66X10^{14}$ molecules cm^{-2} and 1.56 kcal mol^{-1}, respectively. It is not clear why both plots followed the D-R-P theory so well and yet different adsorbate standard states were used.

The error analysis in calculating the values of N_m, ε^2 and B are shown in Appendix III. The maximum error for N_m was 13%, for ε^2 was 1.77%.

Troy[1] obtained linear but separated D-R lines for nitrogen adsorbed on 304 stainless steel at 77, 87, and 90°K. It was suggested that perhaps the separated lines were due to the geometry of the adsorption vessel. Troy's stainless steel adsorption vessel was a straight, large diameter tube. Ideally, for

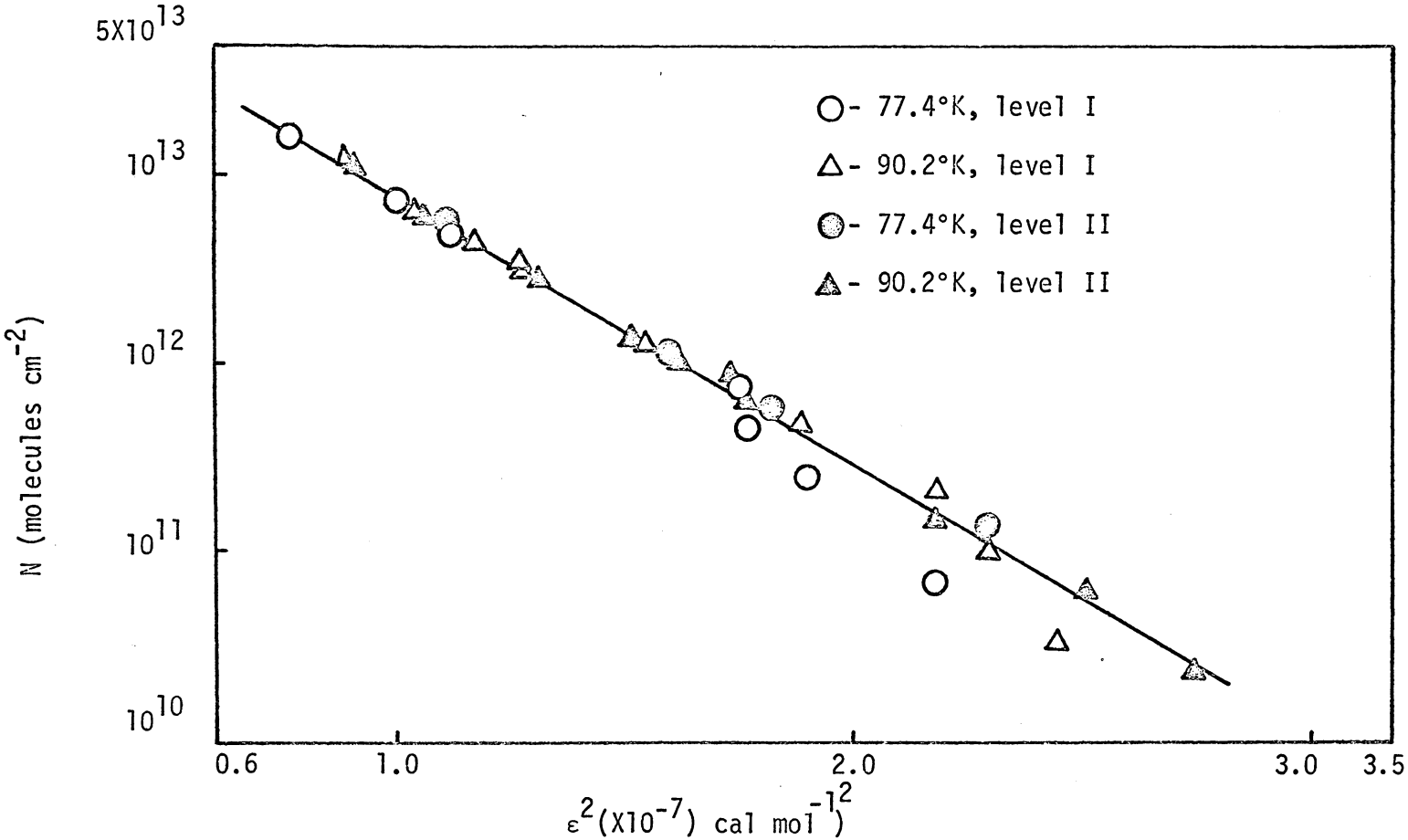

Figure 10. Dubinin-Radushkevich plots for nitrogen on Pyrex by using Equations (1) and (2).

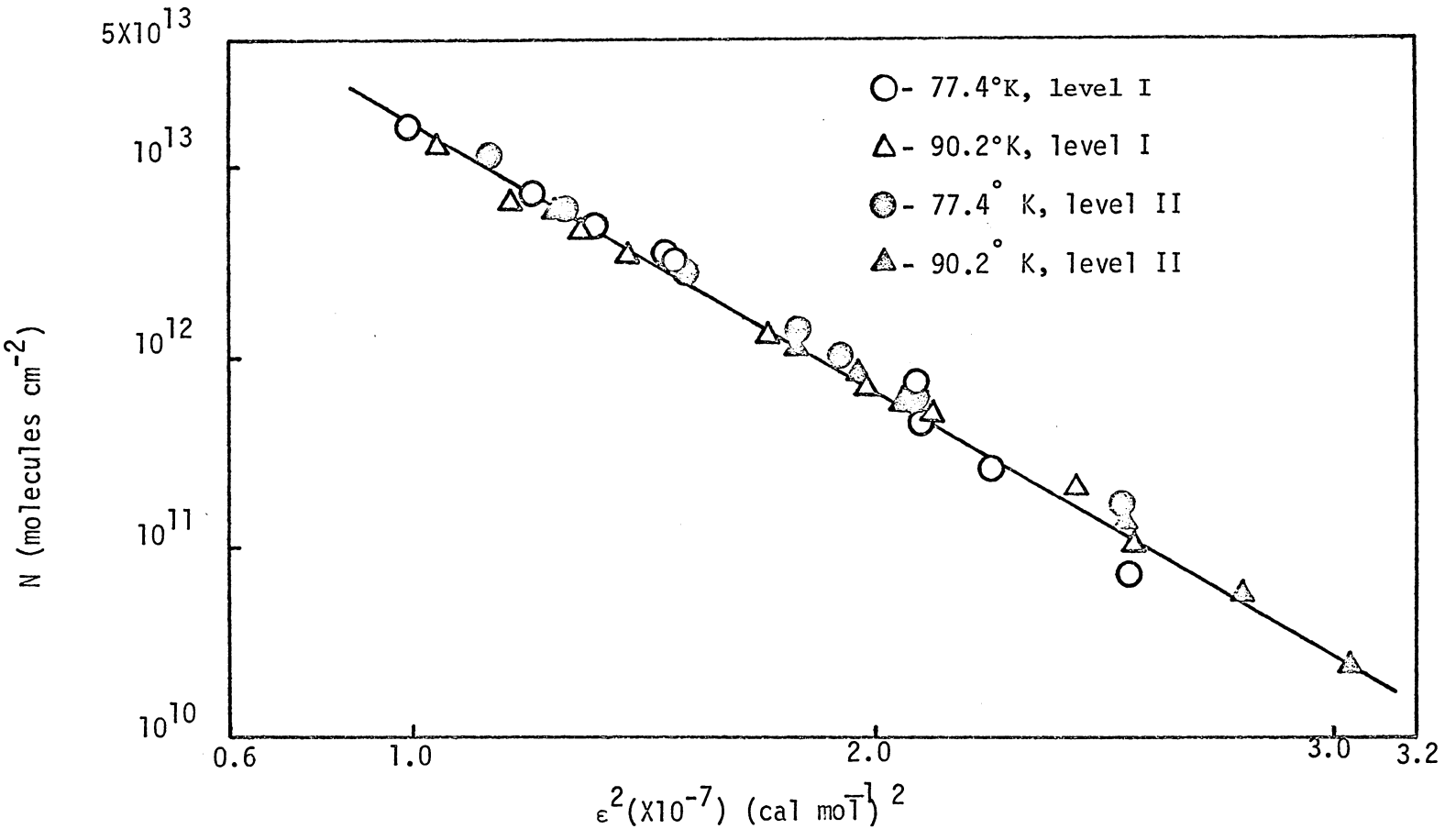

Figure 11. Dubinin-Radushkevich plots for nitrogen on Pyrex by using Equations (1) and (13).

isothermal conditions, the diameter of the adsorption vessel should be large compared to the diameter of the connecting tube. This geometry was not possible in Troy's work. However, in this work the Pyrex finger was constructed specifically to demonstrate the effect of non-isothermal test conditions. Two levels on the Pyrex finger were located at positions having different tube diameters (see Figure 7). If non-isothermal conditions existed inside the finger, different D-R plots might be expected. However, as seen in Figures 10 and 11, the adsorption data from two levels at both temperatures all fell on the same line. Thus, it is concluded that there was no significant non-isothermal effect on the D-R plot for the present system geometry. These results suggest that the separated lines obtained in Troy's work were also not due to non-isothermal conditions in the system.

The adsorption isotherms for the nitrogen/Pyrex system at 77.4°K and 90.2°K are shown in Figure 12. It is generally believed that isotherms should obey Henry's law at low coverages. The angle of the isotherm plotted on the log-log basis should be 45° if Henry's law is obeyed. However, this behavior is not found in this system. The angles of the slopes of the 77.4 and 90.2°K isotherms at the low coverage ends were 32° and 34°, respectively. The general shape of these isotherms is similar to those of Hobson and Armstrong,[2] and of Outlaw.[29] The amount of adsorption was about a factor or two lower than that of Hobson and Armstrong at the

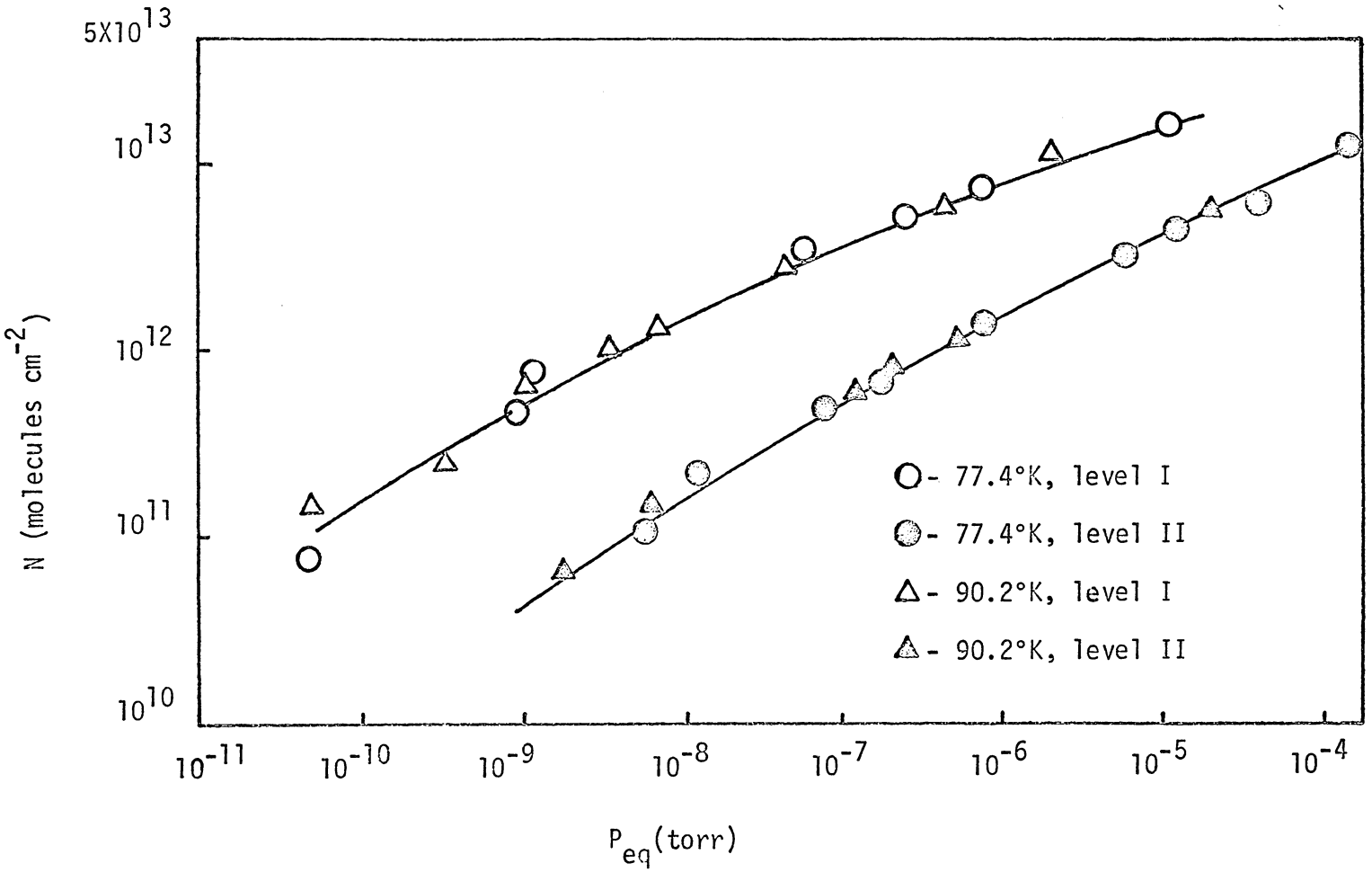

Figure 12. Isotherms of nitrogen on Pyrex.

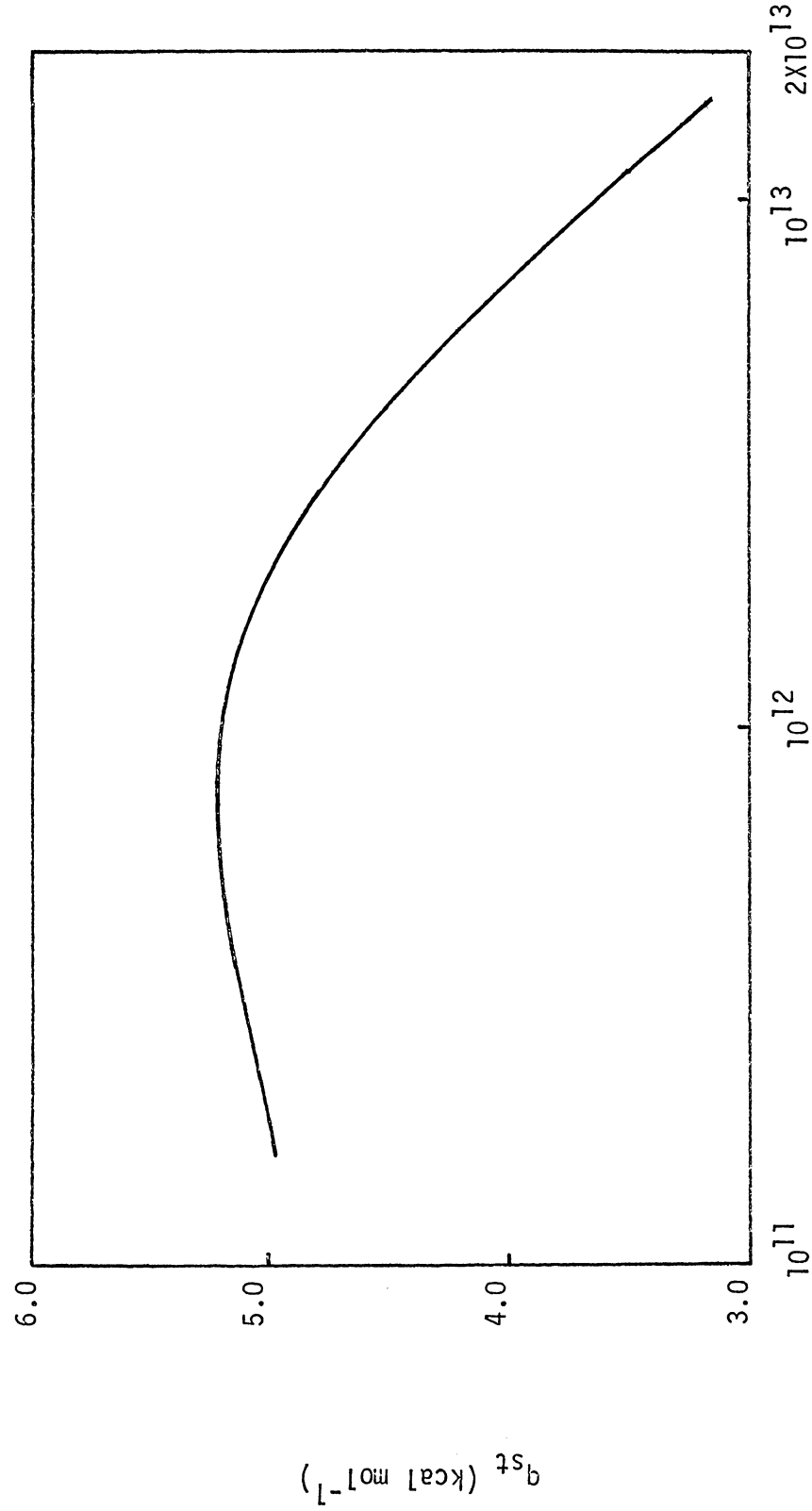

Figure 13. Isosteric heat for nitrogen on Pyrex.

lower pressure end. This is probably due to the background gas interference and ion gauge deviation in the low pressure range. Outlaw found higher isotherms but the Pyrex in his system was chemically leached and more surface area was available for adsorption.

Isosteric heats of adsorption were calculated for the nitrogen/Pyrex system by using Equation (15), and are plotted in Figure 13 as a function of the number of molecules adsorbed. Note that data points are not shown in this figure since the heats were not measured directly but rather calculated. The type of curve shown in Figure 13, a decreasing heat with increasing coverage, indicates the heterogeneous nature of the Pyrex surface. However, at the low coverage end ($N < 8X10^{11}$ molecules cm^{-2}) the heat increased with increasing coverage. This may be due to the uncertainty in the isotherms in the low pressure range as discussed in the Data Analysis chapter. A value of 4.5 kcal mol^{-1} for the isosteric heat was obtained for a value of N of $5X10^{12}$ molecules $cm.^{-2}$ This value was lower than that of Hobson and Armstrong[2] and Outlaw[29] who reported 5.1 and 6.34 kcal mol,$^{-1}$ respectively, at the same number of nitrogen molecules adsorbed per unit area. The difference may be due to different surface pre-treatments, such as the time and the temperature of annealing, and the surface cleaning. For example, in Outlaw's work, the Pyrex surface was leached chemically prior to adsorption measurements.

The D-R plots of argon adsorbed on Pyrex at 77.4, 81.8, 88.1 and 90.2°K, and at different levels are given in Figures 14, 15 and 16. These are the first results that have been reported for argon adsorbed at low pressures on Pyrex over the temperature range 77.4 to 90.2°K. The results plotted in Figure 14 were calculated from Equations (1) and (2), and the vapor pressure of solid argon was used for P_o. The plots in Figure 15 were also based on Equations (1) and (2) but the vapor pressure of liquid argon was used for P_o. Straight but separated lines which do not obey the temperature-invariant property that the D-R-P theory predicts are seen in the above two figures. Note that the use of different values of P_o do not change this conclusion.

The results plotted in Figure 16 were calculated using Equations (1) and (13). In this case, a temperature-independent, straight D-R line is obtained, which indicates that Equations (1) and (13) do indeed give better D-R results for argon adsorbed on Pyrex than Equations (1) and (2). This is a major point of this thesis. Dubinin and Nikolaev[41] used Equation (13) for nitrogen, xenon, tetrafluoroethylene and hexafluoropropylene adsorbed on active carbon at high pressures and at temperatures above the critical point of the adsorbates. There has not been to date a reference to the use of Equations (1) & (13) in analyzing low pressure adsorption data. All workers in this area have used Equation (2), which, as seen above can lead to separated D-R lines rather than a coincident D-R line.

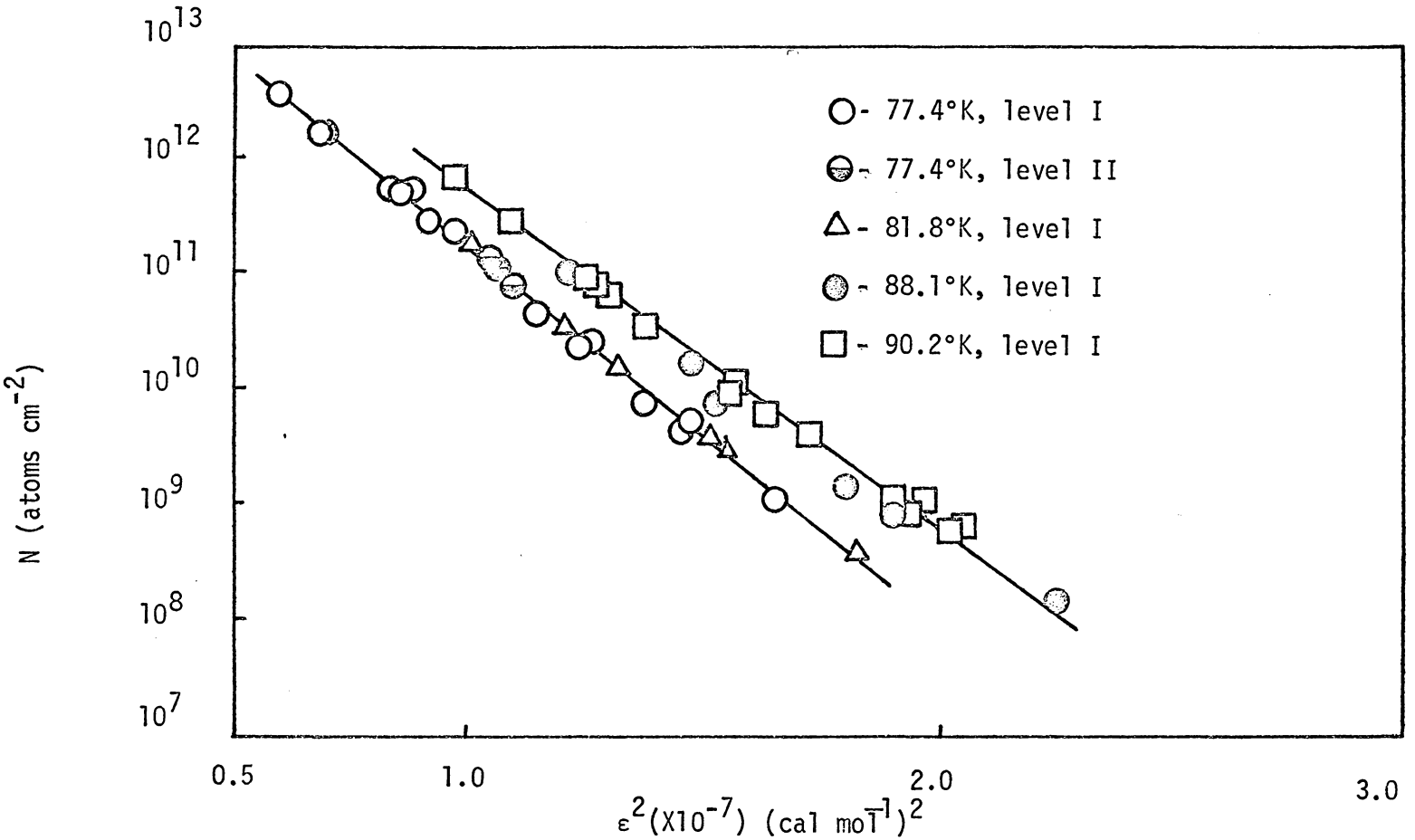

Figure 14. Dubinin-Radushkevich plots for argon on Pyrex by using Equations (1) and (2).

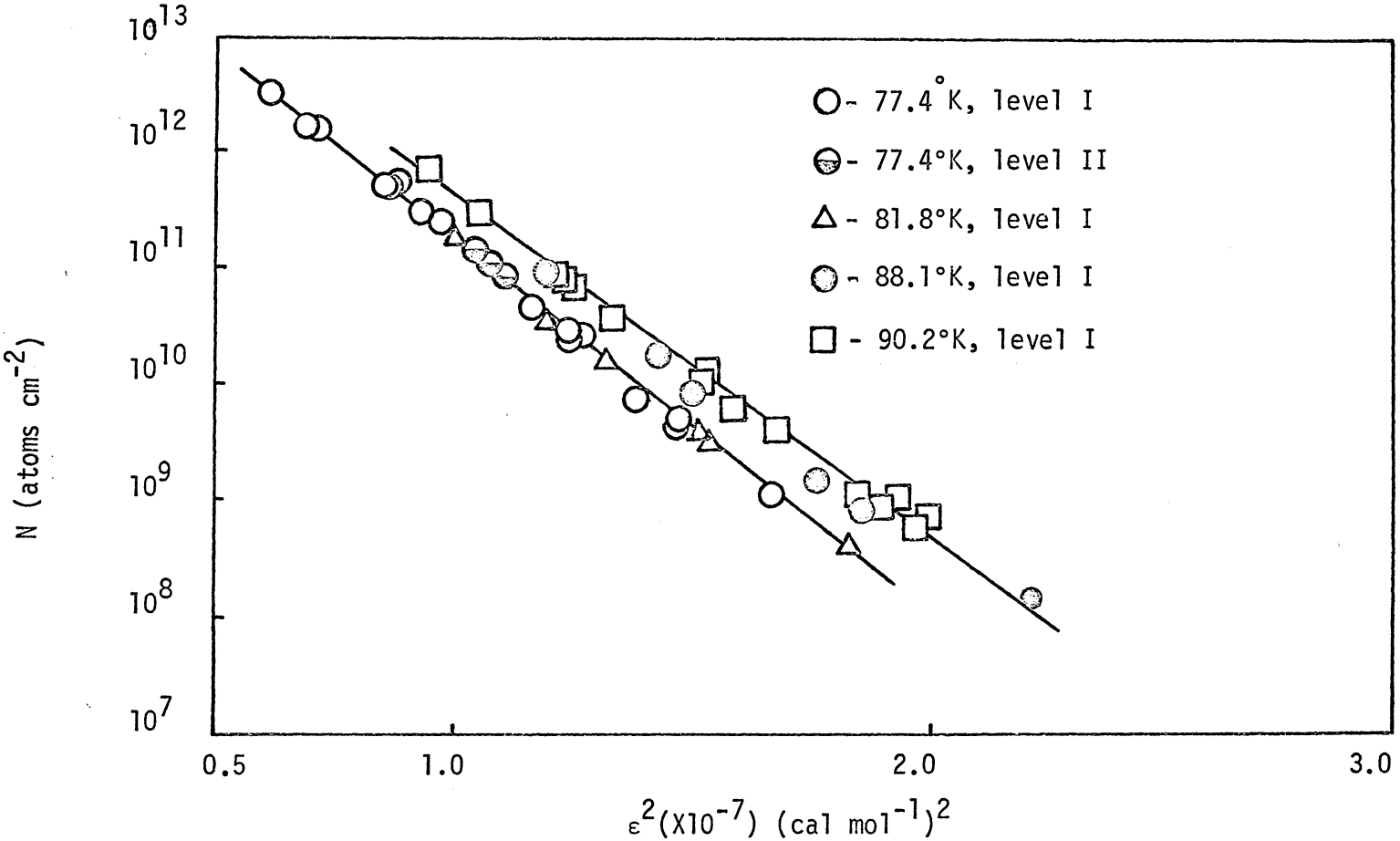

Figure 15. Dubinin-Radushkevich plots for argon on Pyrex based on Equations (1) and (2).

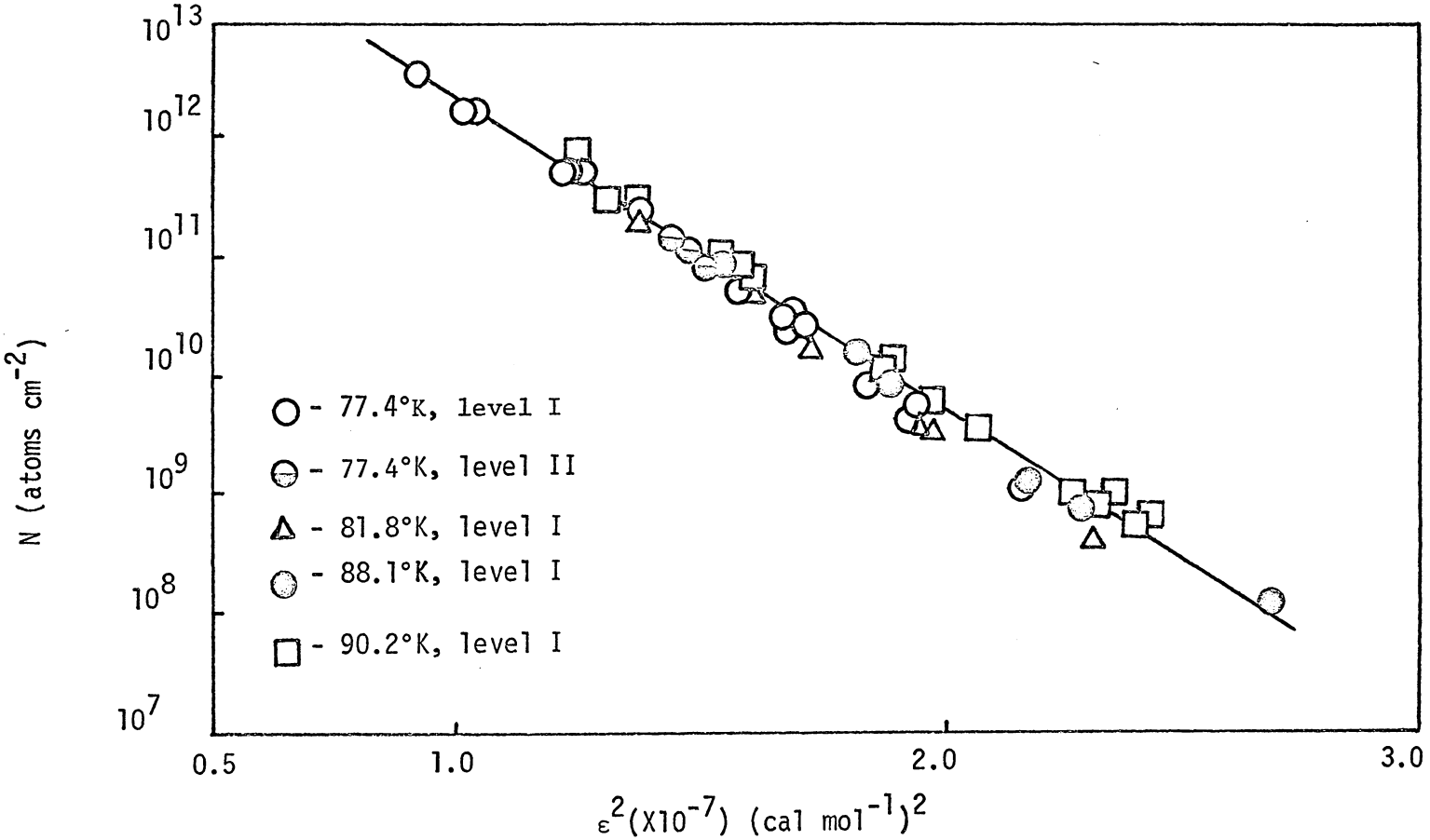

Figure 16. Dubinin-Radushkevich plots for argon on Pyrex by using Equations (1) and (13).

Further, from Figures, 14, 15 and 16, the data obtained at different levels on the finger but at the same temperature fell on the same line, as was the case for nitrogen adsorbed on Pyrex. This is additional evidence that separated D-R plots are not caused by the system geometry in the present apparatus.

Isotherms at four temperatures for the argon/Pyrex system are given in Figure 17. The general shape of the isotherms is the same as those of others.[2,30] The slopes of the lower coverage ends of the isotherms increased from 41 to 43, to 44, to 44°, as the adsorption temperature increased from 77.4 to 90.2°K. The trend of increasing slopes indicates that for the argon/Pyrex system Henry's law behavior is approached at the higher temperature. This conclusion has not been stated before in the literature.

Isosteric heats of adsorption for this system are shown in Figure 18. Generally, these curves again indicate the heterogeneity of the Pyrex surface the heat decreasing with increasing surface coverage. The increase in the isosteric heats with increasing coverage at the low coverage ends of 77.4 to 81.8° K curve and 88.1 to 90.2°K curve are presumably due to the uncertainities in the isotherm measurements as discussed previously.

It is common practice to calculate isosteric heats of adsorption based on isotherms obtained at only two temperatures.[88] However, Young and Crowell[13] cautioned that if a transition occurs in the adsorbed phase then the use of only two isotherms is invalid. If

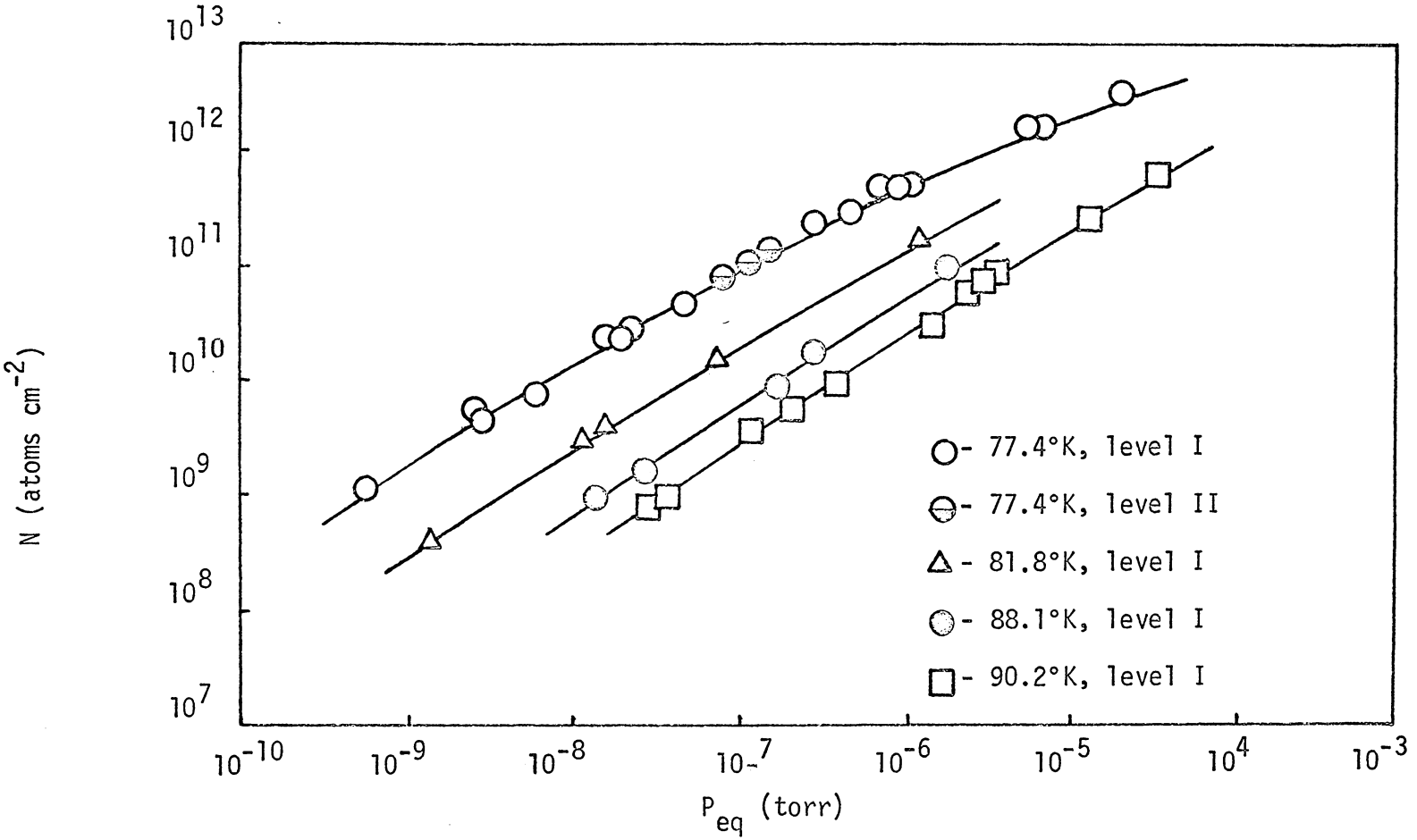

Figure 17. Isotherms for argon on Pyrex.

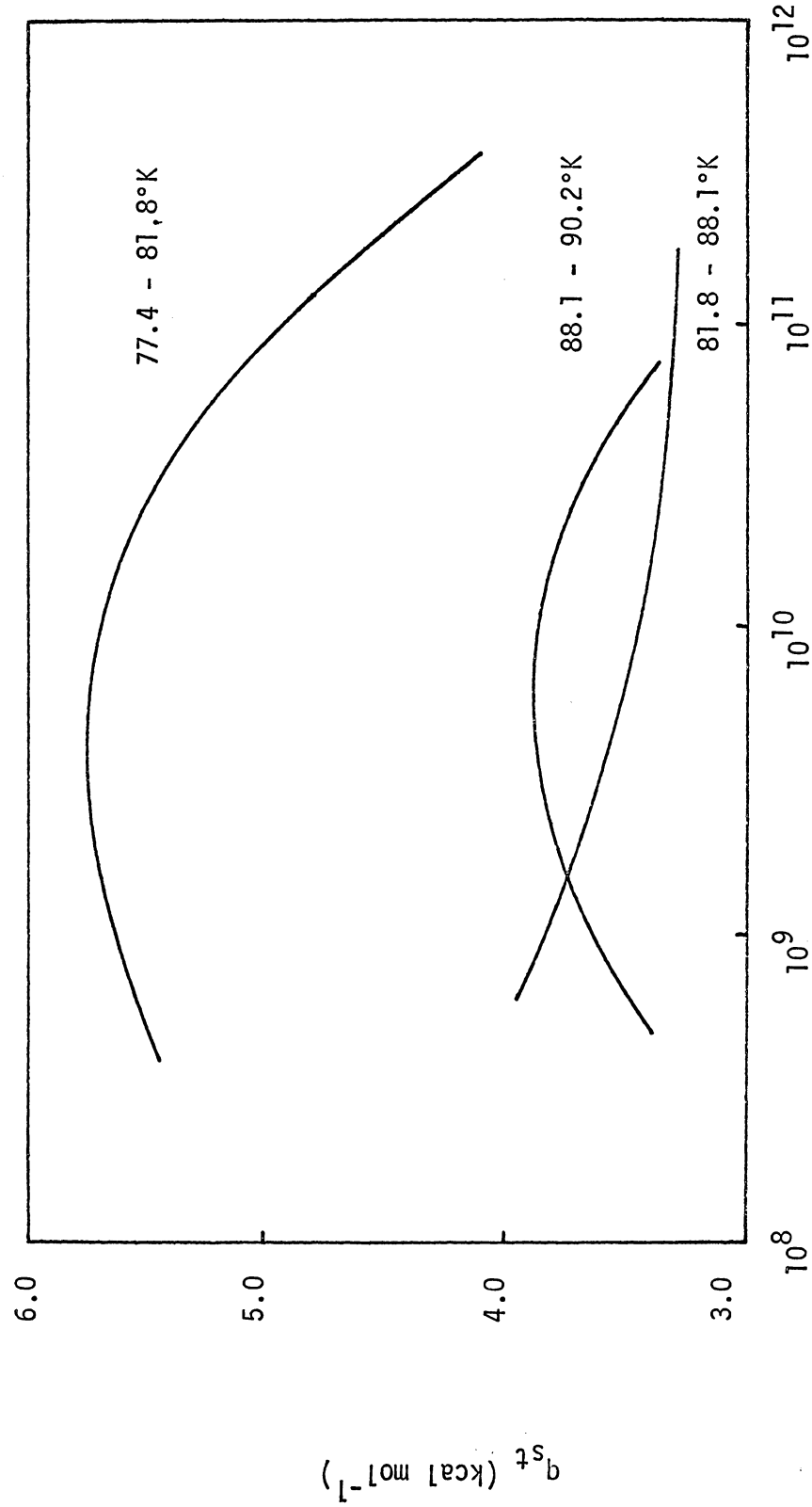

Figure 18. Isosteric heat for argon on Pyrex.

the argon/Pyrex system were well-behaved, the calculated isosteric heat should be independent of the adsorption temperature. However, as seen in Figure 18, different temperature ranges give different isosteric heats. The curves in Figure 18 are significantly different. The error analysis shown in Appendix III indicates a maximum error of 15% in the values of the isosteric heat which is clearly much less than the differences seen in Figure 18. It is concluded that the state of the adsorbed phase was continuously changing as a function of the adsorption temperature. This supports the use of Equation (13) which characterizes the adsorbed state by the relation $P^o = \tau^2 P_c$ where clearly P^o is a function of the adsorption temperature.

At an adsorption coverage of $1X10^{11}$ atoms cm^{-2} a q_{st} value of 4.95 kcal mol^{-1} for the temperature range 77.4 to 81.8°K can be compared to the value of 4.5 kcal mol^{-1} obtained by Hobson and Armstrong[2] in the temperature range 63.3 to 77.4°K. The agreement is reasonably good.

2. Iron

The following results are the first results that have been reported on the adsorption of nitrogen, argon and krypton on as received and chemically cleaned iron surfaces at low pressures.

The D-R plots of argon adsorbed on iron before and after the Diversey process are given in Figures 19 and 20. The original D-R-P theory based on Equation (2) again gives separated linear plots as seen in Figure 19. The modified D-R-P theory based on Equation (13)

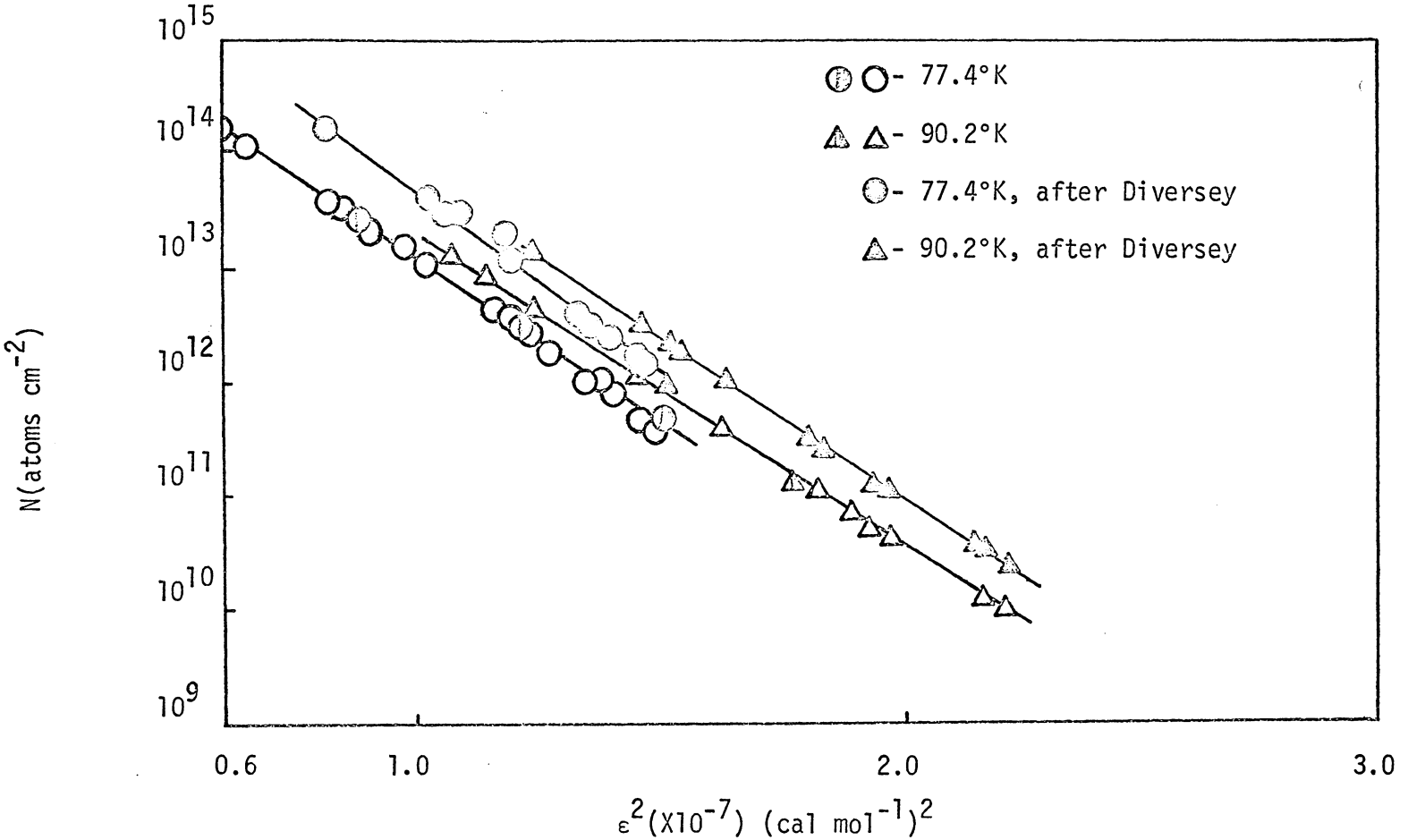

Figure 19. Dubinin-Radushkevich plots for argon on iron, by using Equations (1) and (2), and saturated liquid argon vapor pressure for P_o.

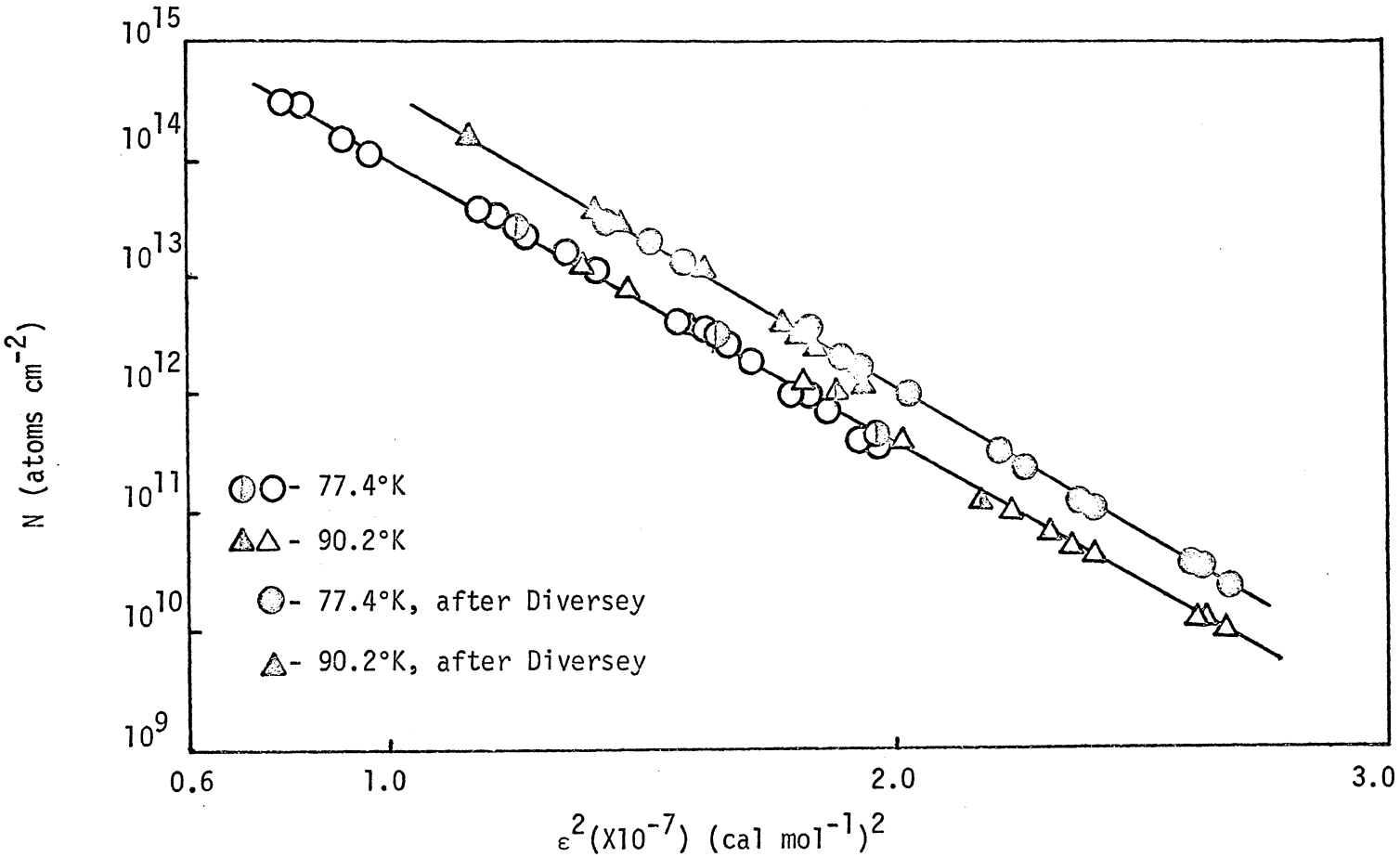

Figure 20. Dubinin-Radushkevich plots for argon on iron, by using Equations (1) and (13).

gives a single linear plot as shown in Figure 20. The half darken symbols (◐ and ◭) were data points taken several months later during a series of adsorption measurements of other gases. Clearly, these plots indicate that the iron surface was not changed as far as the adsorption of argon is concerned, and hence the adsorption data are quite reproducible.

Isotherms of the argon/iron system are shown in Figure 21. The isotherms obtained after the Diversey process were shifted towards greater adsorption, but the general shape remained the same as that before the cleaning process. The slopes at 77.4 and 90.2°K are 44 and 52° for the iron surface before the Diversey process, and 44 and 48° for the surface after the Diversey process. The fact that the angles exceeded 45° (Henry's law) may be due to the inaccuracy of isotherm measurements at low pressures.

The isosteric heats of the argon/iron system are plotted as a function of number of atoms adsorbed in Figure 22. Apparently, the iron surface was not as heterogeneous as the Pyrex surface and had less heterogeneity after the Diversey process as indicated by the nearly constant value of isosteric heat. Presumably, this was due to the formation of a uniform surface oxide layer and less surface contamination.

The isosteric heats of argon adsorbed on iron before the Diversey process ranged from 4.5 to 4.3 kcal mol^{-1} within the adsorption coverages, θ, from $1.5X10^{-5}$ to $3X10^{-4}$. This range of θ values correspond to a range of N values from $5X10^{11}$ to $1X10^{13}$

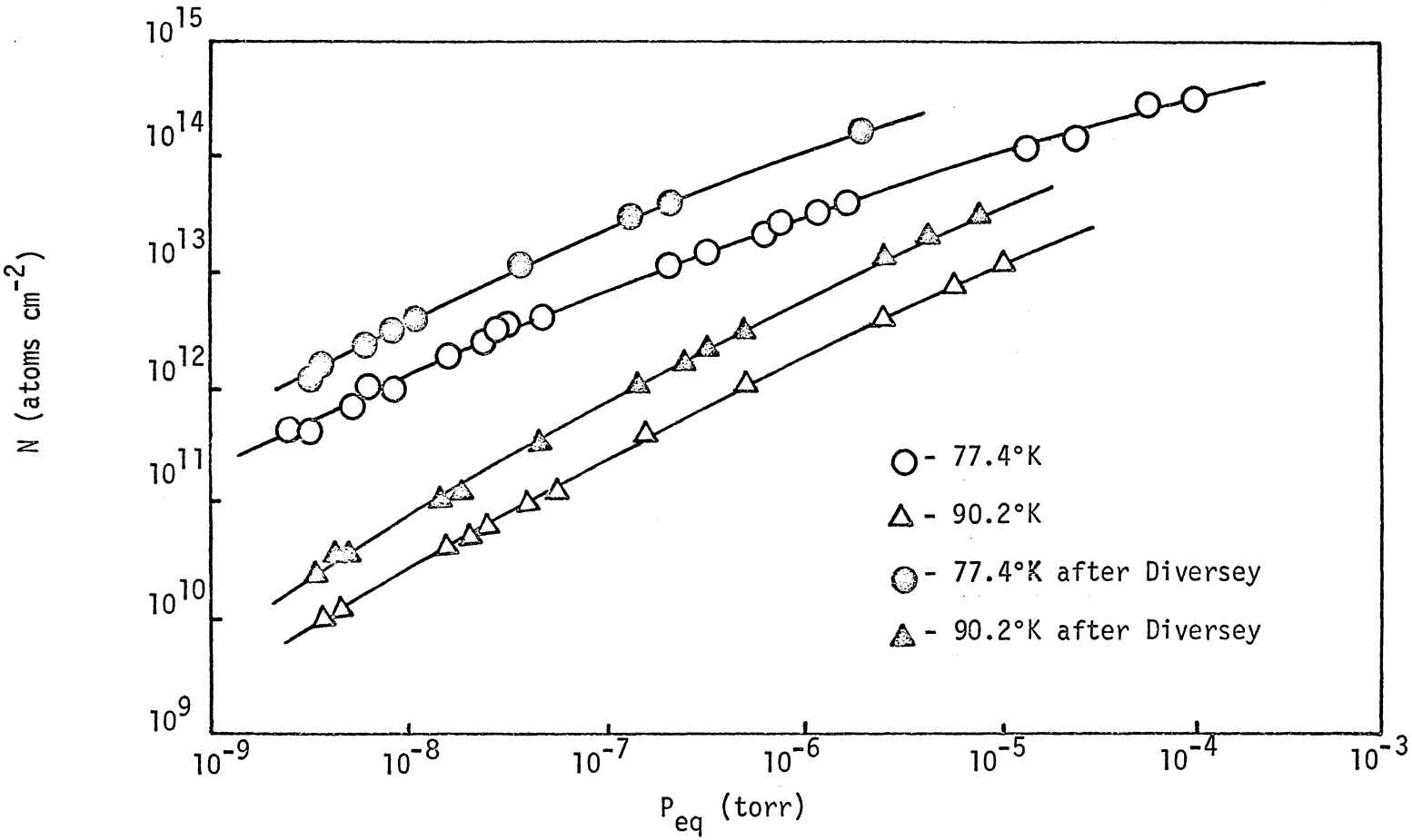

Figure 21. Isotherms for argon on iron.

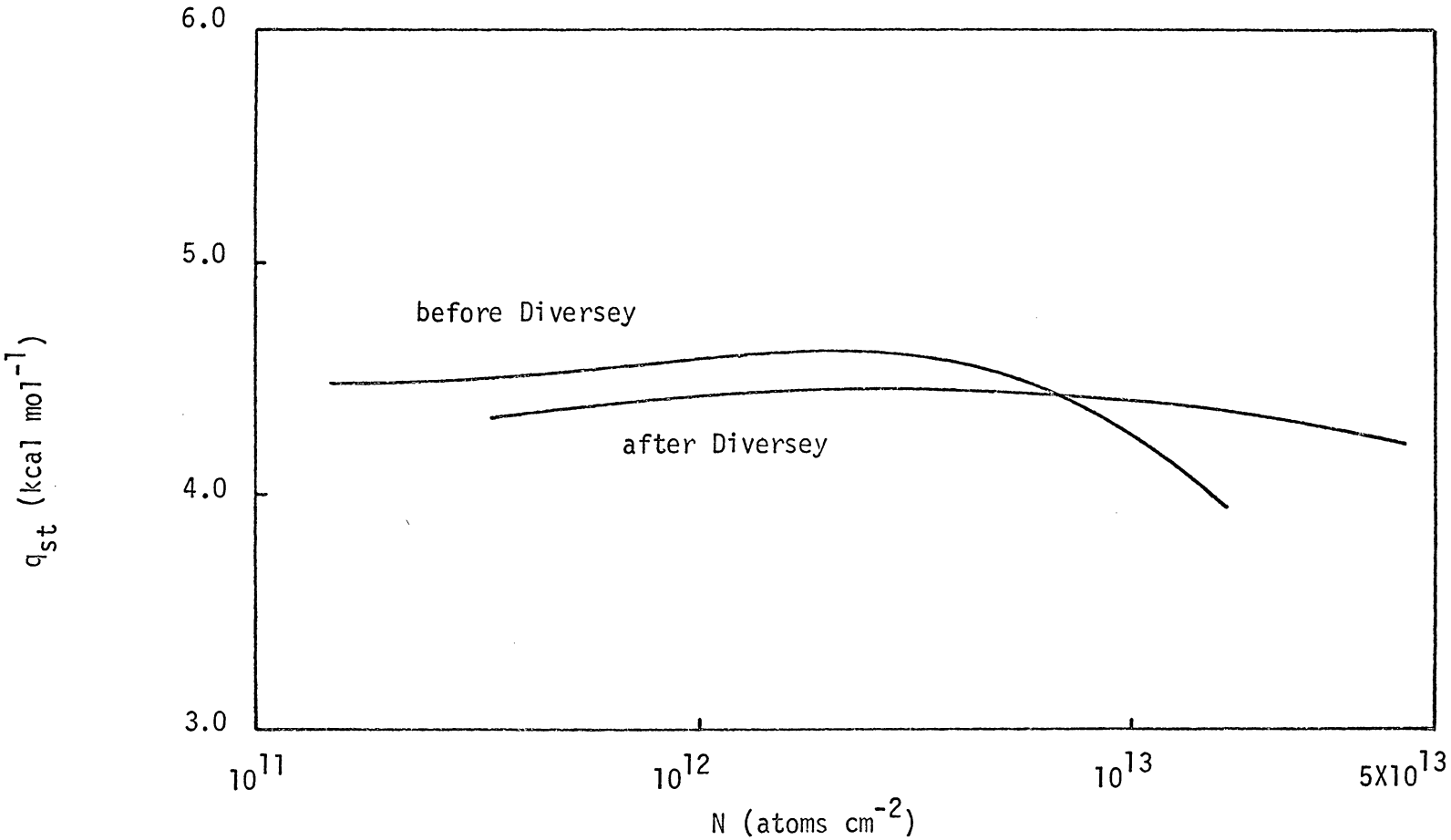

Figure 22. Isosteric heat for argon on iron.

atoms $cm.^{-2}$. The isosteric heats of argon adsorbed on iron after the Diversey process were close to a constant value of 4.3 kcal mol^{-1} within the coverages from $4X10^{-6}$ to $8X10^{-5}$. This range of θ values correspond to a range of N values from $5.2X10^{11}$ to $1X10^{13}$ atoms $cm.^{-2}$. There is no comparable literature data available. Hall and Hope[34] found that isosteric heats for argon adsorbed on iron film ranged from 1.8 to 3.6 kcal mol^{-1} for surface coverage 0.1 to 0.25.

Stainless steel is approximately 70% iron, and it is of interest to compare the present data to data obtained for stainless steel. Troy and Wightman[11] found that isosteric heats of argon adsorbed on 304 stainless steel ranged from 5.8 to 4.6 kcal mol^{-1} for coverages from 0.0001 to 0.01. The isosteric heats of the present work agree reasonably well with the above values. This is reasonable since oxide layers exist on both surfaces (see Reference (1) and next section).

The D-R plot of nitrogen adsorbed on iron based on Equations (2) and (13) are given in Figures 23 and 24, respectively. Again, the modified theory gave better results. The isotherms of this system are plotted in Figure 25. The isotherms after the Diversey process remained similar in shape to those obtained before the Diversey process. However, the isotherms were shifted to higher adsorption after the Diversey process. Henry's law behavior was not observed in this system.

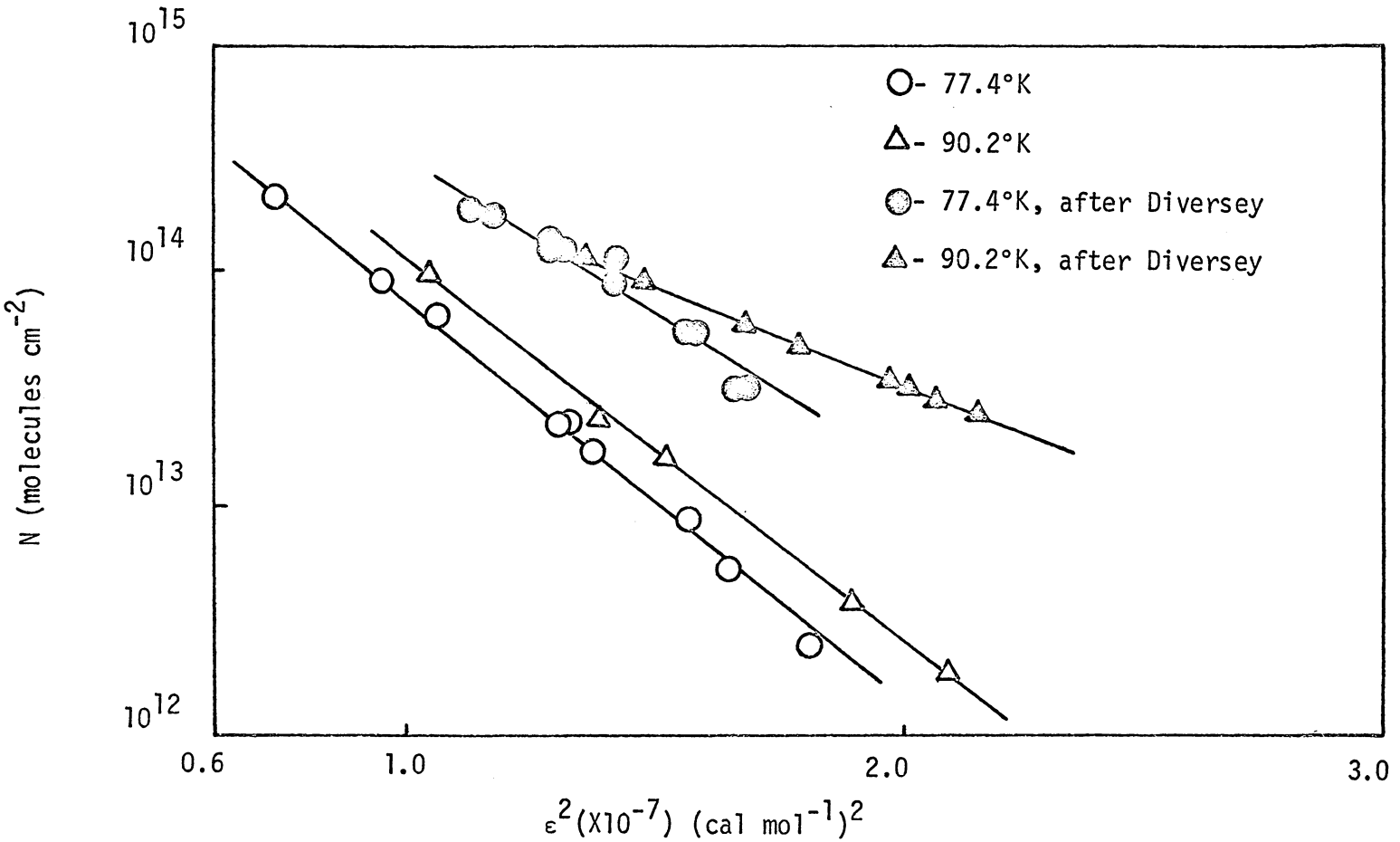

Figure 23. Dubinin-Radushkevich plots for nitrogen on iron, by using Equations (1) and (2), and saturated liquid nitrogen vapor pressure for P_o.

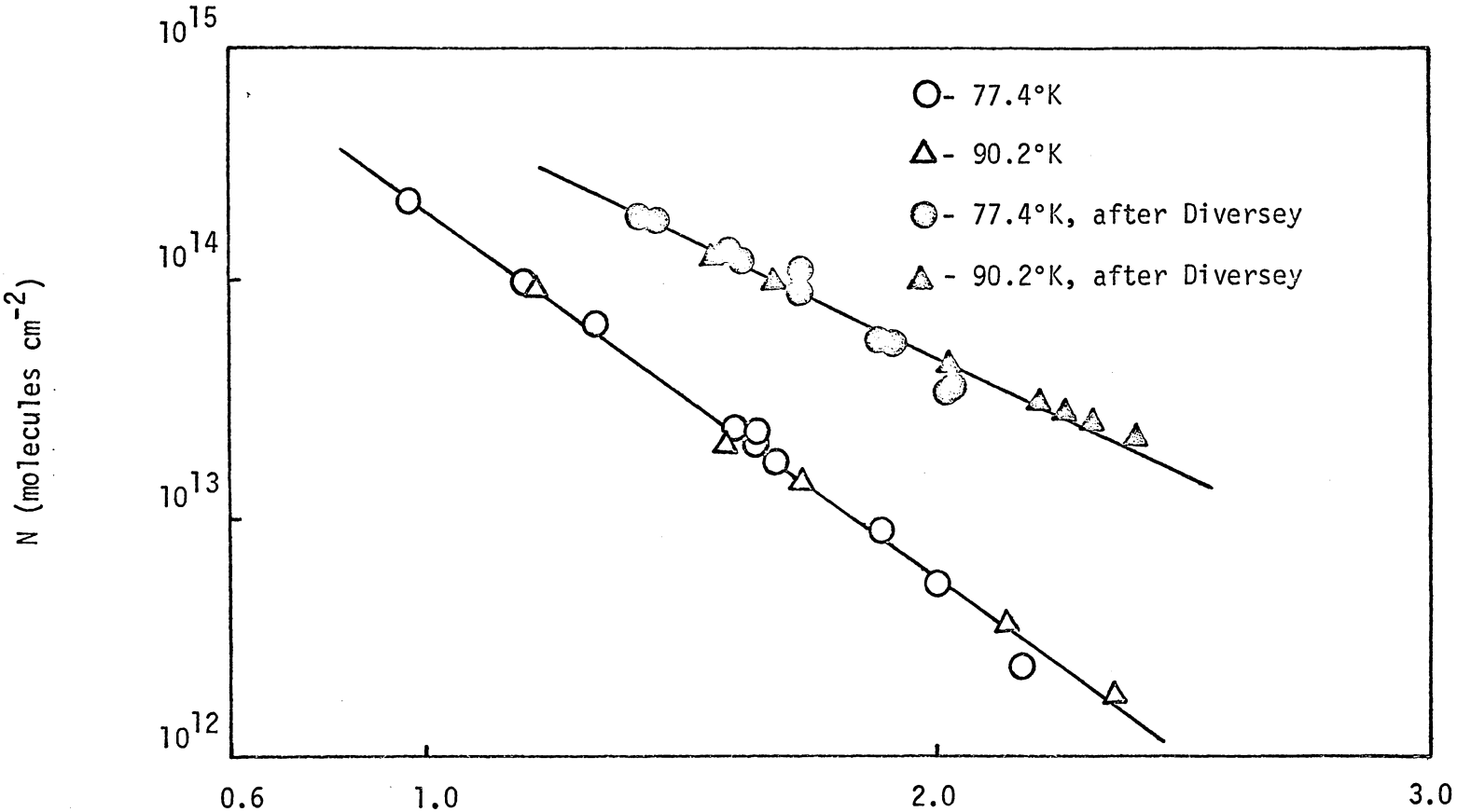

Figure 24. Dubinin-Radushkevich plots for nitrogen on iron, by using Equations (1) and (13).

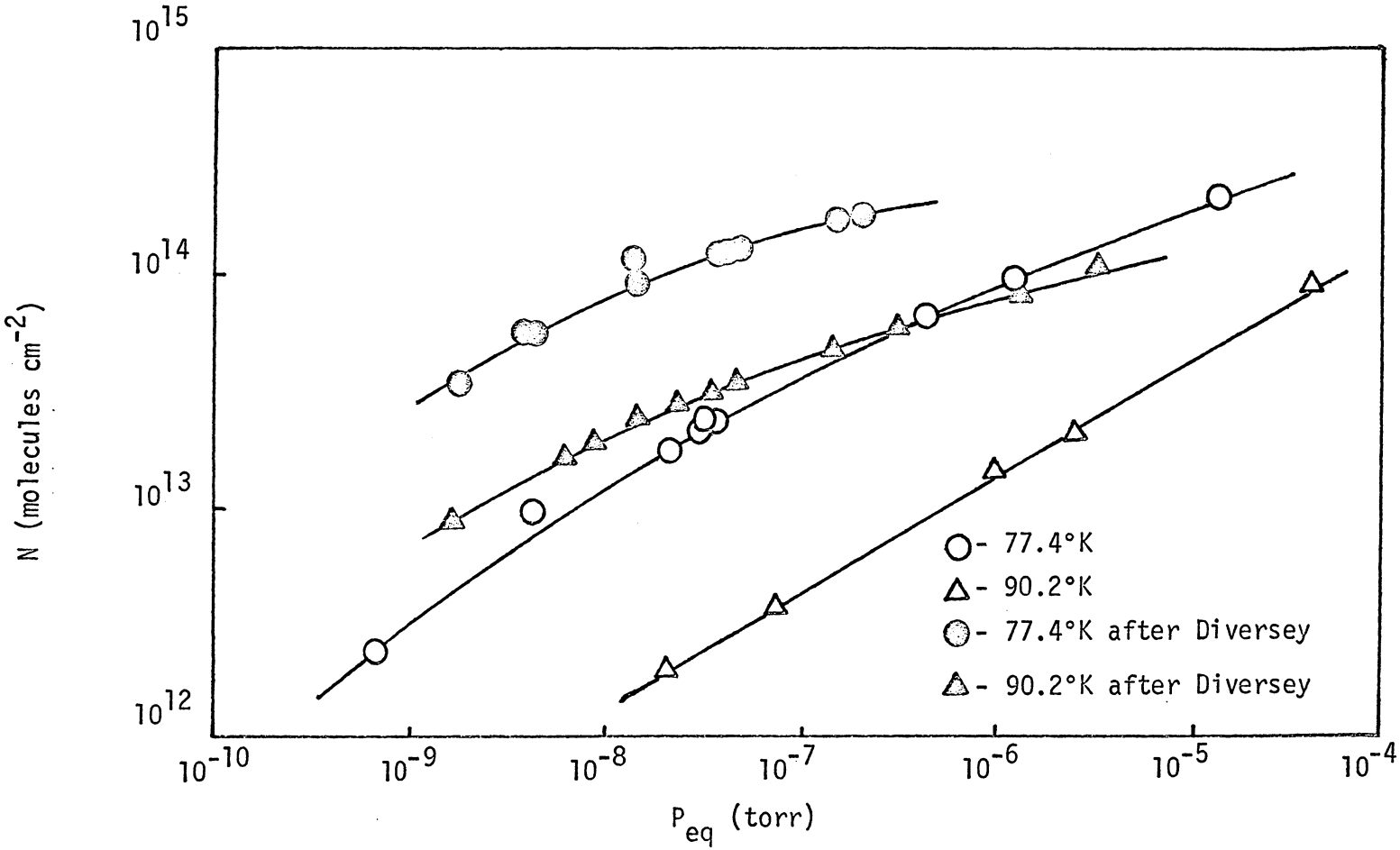

Figure 25. Isotherms for nitrogen on iron.

Isosteric heats of the nitrogen/iron system are shown in Figure 26. The isosteric heat curve before the Diversey process was similar to those of the argon/iron system. But the isosteric heat after the Diversey process was increased as the surface coverage increased. This type of shape for an isosteric heat curve usually reflects a low energy surface, which is totally different conclusion from that reached for the argon/iron system. This behavior is not understood since metal and metal oxide surfaces are generally considered to be heterogeneous in nature and have rather high surface energies. Hall and Hope[34] reported the isosteric heats of nitrogen adsorbed on iron film ranged from 2.4 to 1.7 kcal mol^{-1} for surface coverages from 0.007 to 0.3, and the isosteric heats of nitrogen adsorbed on iron sponge ranged from 1.6 to 2.4 kcal mol^{-1} for surface coverages from 0.03 to 0.3. The interesting point here is that, similar to the present study, the isosteric heat for nitrogen adsorbed on iron film also increased as the surface coverage increased. No explanation was given for their observation. Outlaw[29] studied the adsorption of nitrogen on 347 stainless steel surfaces cleaned by electron impact desorption and by oxygen exposure. For the case of electron desorbed surface, the isosteric heats obtained ranged from 7.25 to 5.5 kcal mol^{-1} over the adsorption range from $3X10^{13}$ to $7X10^{13}$ molecules $cm.^{-2}$ For the case of an oxygen exposed surface, the isosteric heats found ranged from 6.5 to 6 kcal mol^{-1} over the adsorption range from $1X10^{13}$ to $4X10^{13}$ molecules $cm.^{-2}$ Troy and

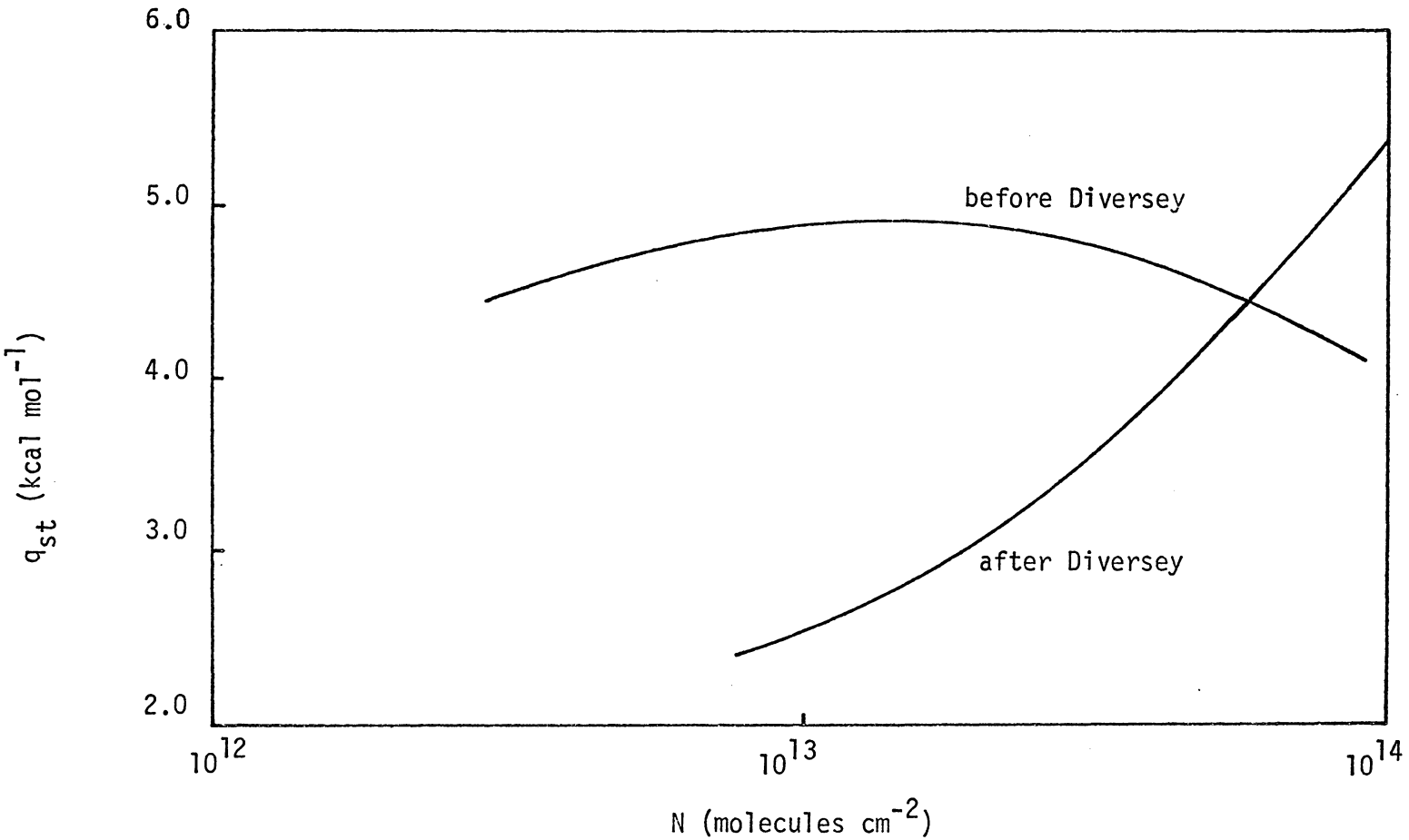

Figure 26. Isosteric heat for nitrogen on iron.

Wightman[89] obtained a value of 4.4 kcal mol^{-1} for the isosteric heat for the nitrogen/304 stainless steel system that varied little with surface coverage from 0.025 to 0.08. This value should be compared to the values of nitrogen adsorbed on iron before the Diversey process for the present study which ranged from 5 to 4 kcal mol^{-1} over the surface coverage range from 0.0016 to 0.16. The agreement between the present results and those of Troy and Wightman is good, even though different adsorbents were used. This is presumably due to the fact that both surfaces were considered mainly to be oxide in nature as discussed previously. However, the heat obtained by Outlaw was high compared to the above values. This was the consequence of the surface treatments as explained by Outlaw.

Outlaw[29] has also studied the adsorption of nitrogen on nickel, which is another component of stainless steel. He obtained a small invariant isosteric heat of about 5.7 kcal mol^{-1} for nitrogen adsorbed on nickel cleaned by electron impact desorption. A slightly changed value of 5.3 kcal mol^{-1} was obtained for nitrogen adsorbed on an oxygen treated nickel surface. It would be of interest to compare the present data for iron, Outlaw's results on nickel, and work on chromium to the results of stainless steel. Unfortunately, no work has been reported for nitrogen adsorbed on chromium.

The D-R plots of krypton adsorbed on iron before and after the Diversey process are given in Figures 27 and 28 based on Equations (2) and (13), respectively. Again, for this system the modified theory

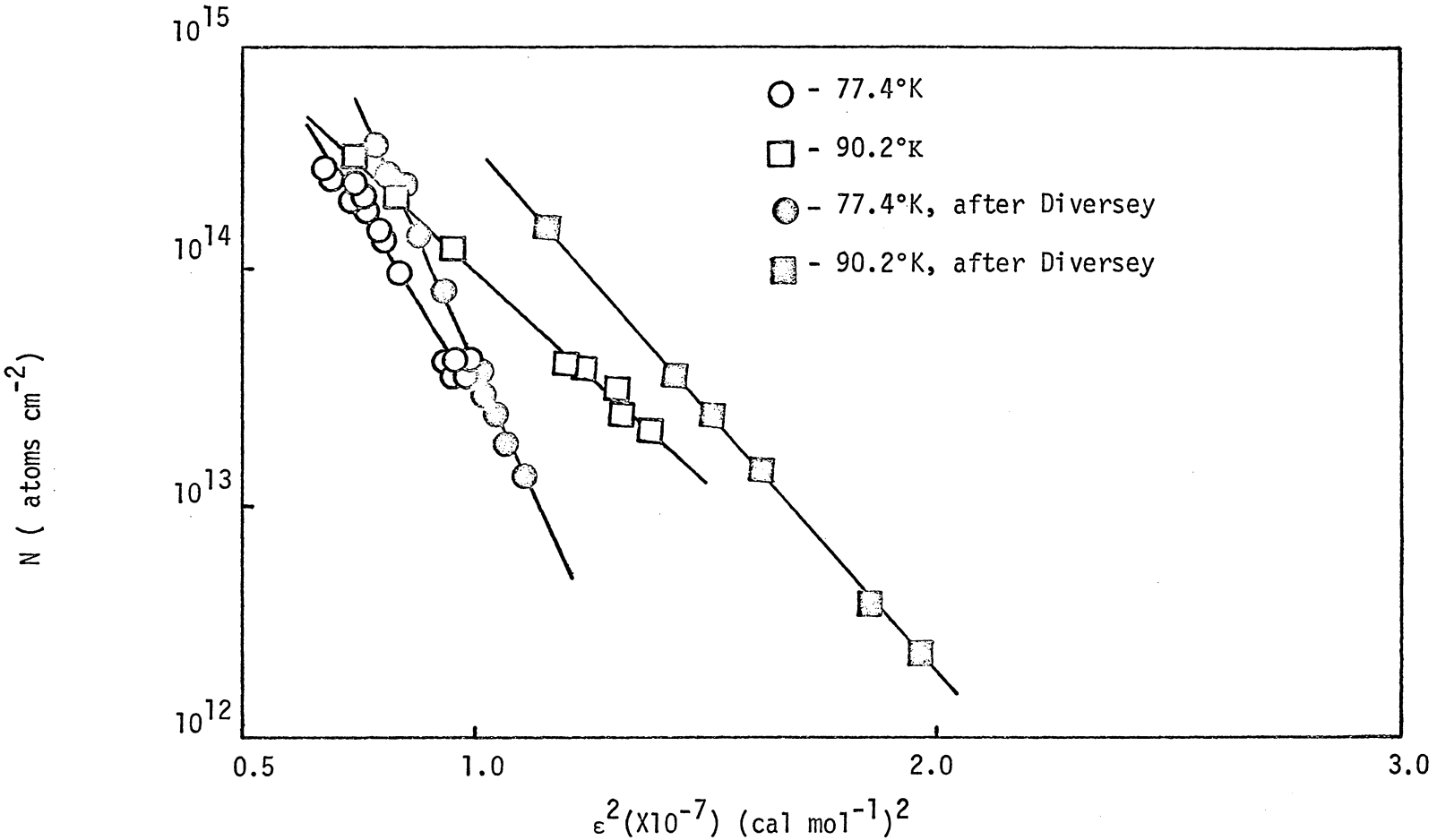

Figure 27. Dubinin-Radushkevich plots for krypton on iron by using Equations (1) and (2), and saturated liquid krypton vapor pressure for P_o.

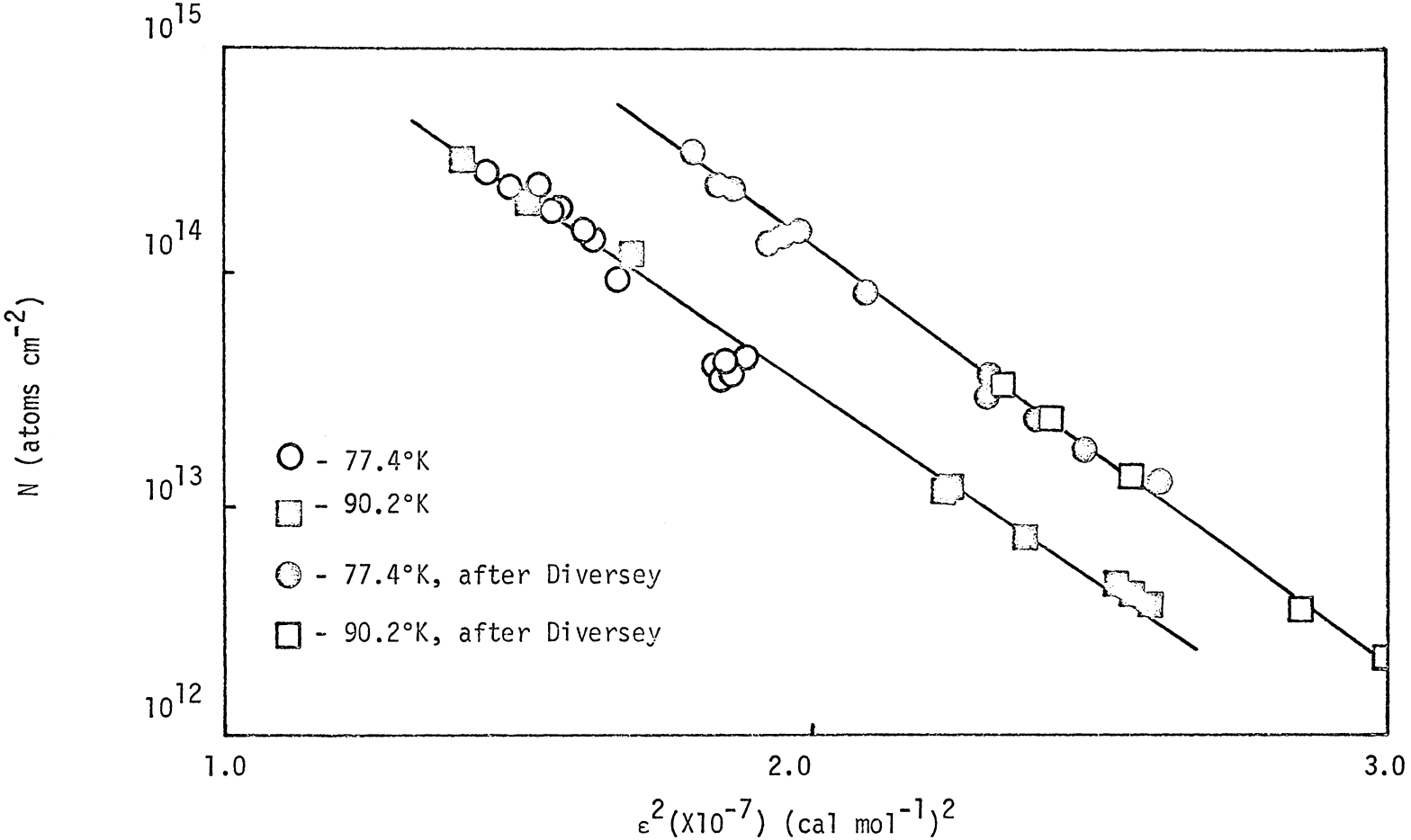

Figure 28. Dubinin-Radushkevich plots for krypton on iron, by using Equations (1) and (13).

gave better results. The isotherms are plotted in Figure 29. Similar to the case of the nitrogen/iron system, the isotherms after the Diversey process retained the similar shape but were shifted to higher adsorption. Henry's law behavior was not observed for this system either.

The isosteric heats for the krypton/iron system are shown in Figure 30 as a function of the number of atoms adsorbed. Similar to the case of nitrogen adsorbed on iron after the Diversey process, both isosteric heat increase as the surface coverage is increased. This is not understood, since the iron surface is generally believed to be a heterogeneous high energy surface.

Hall and Hope[34] obtained a value for the isosteric heat of 2.4 kcal mol^{-1} at a coverage of 0.1 for krypton adsorbed on iron film and a range of isosteric heat values from 1.9 to 3.1 kcal mol^{-1} for the coverage range from 0.1 to 0.8 for krypton adsorbed on iron sponge. Values of the isosteric heat for the present study are a little larger than the above values. However, the present study was in the low surface coverage region while Hall and Hope's work was done at higher coverages.

The isosteric heats of argon, nitrogen and krypton adsorbed on iron before and after the Diversey process (see Figures 22, 26 and 30), are all small compared to the heats of chemisorption.[31] For example the heat of adsorption for nitrogen chemisorbed on tungsten was 95 kcal mol^{-1}. Thus, it is concluded that argon

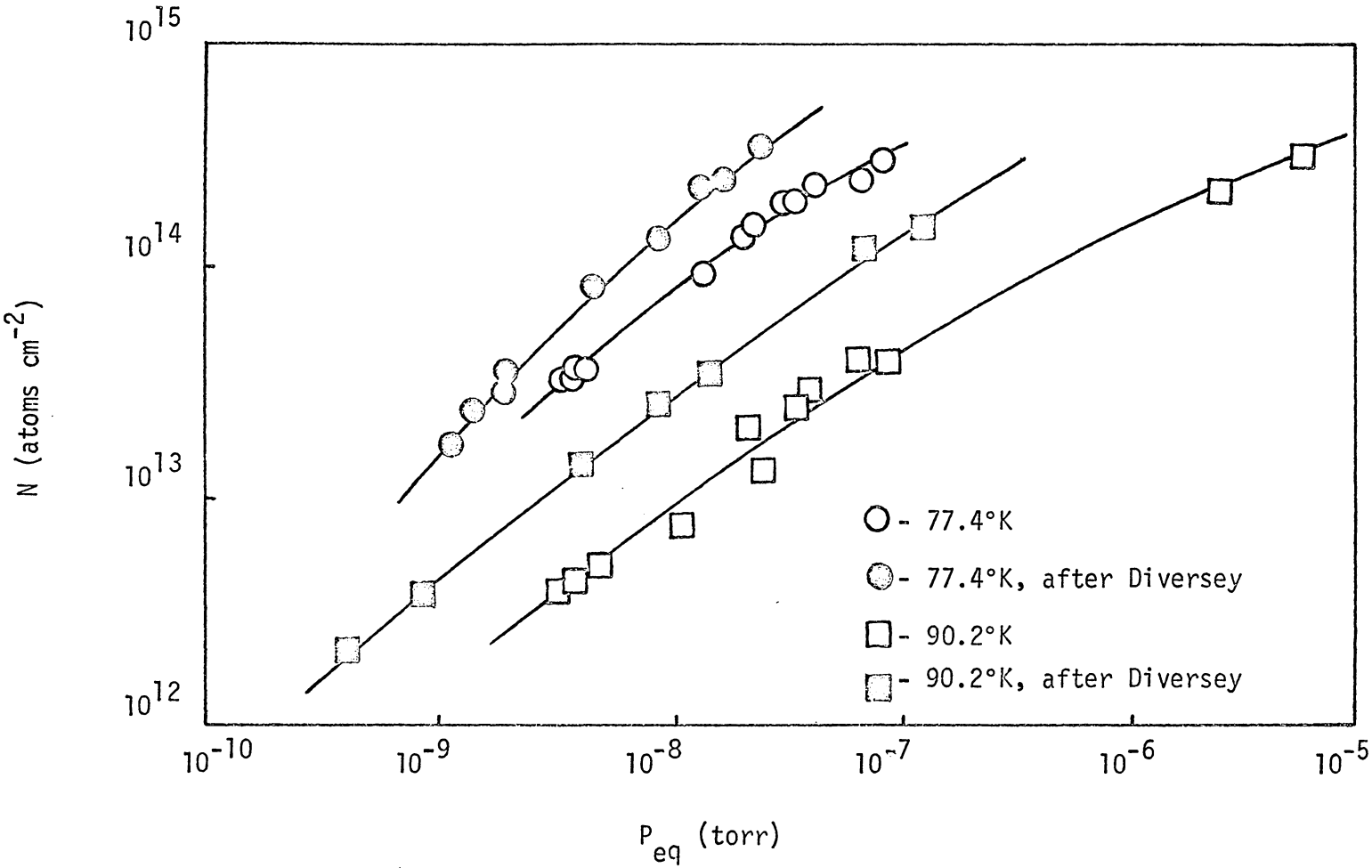

Figure 29. Isotherms for krypton on iron.

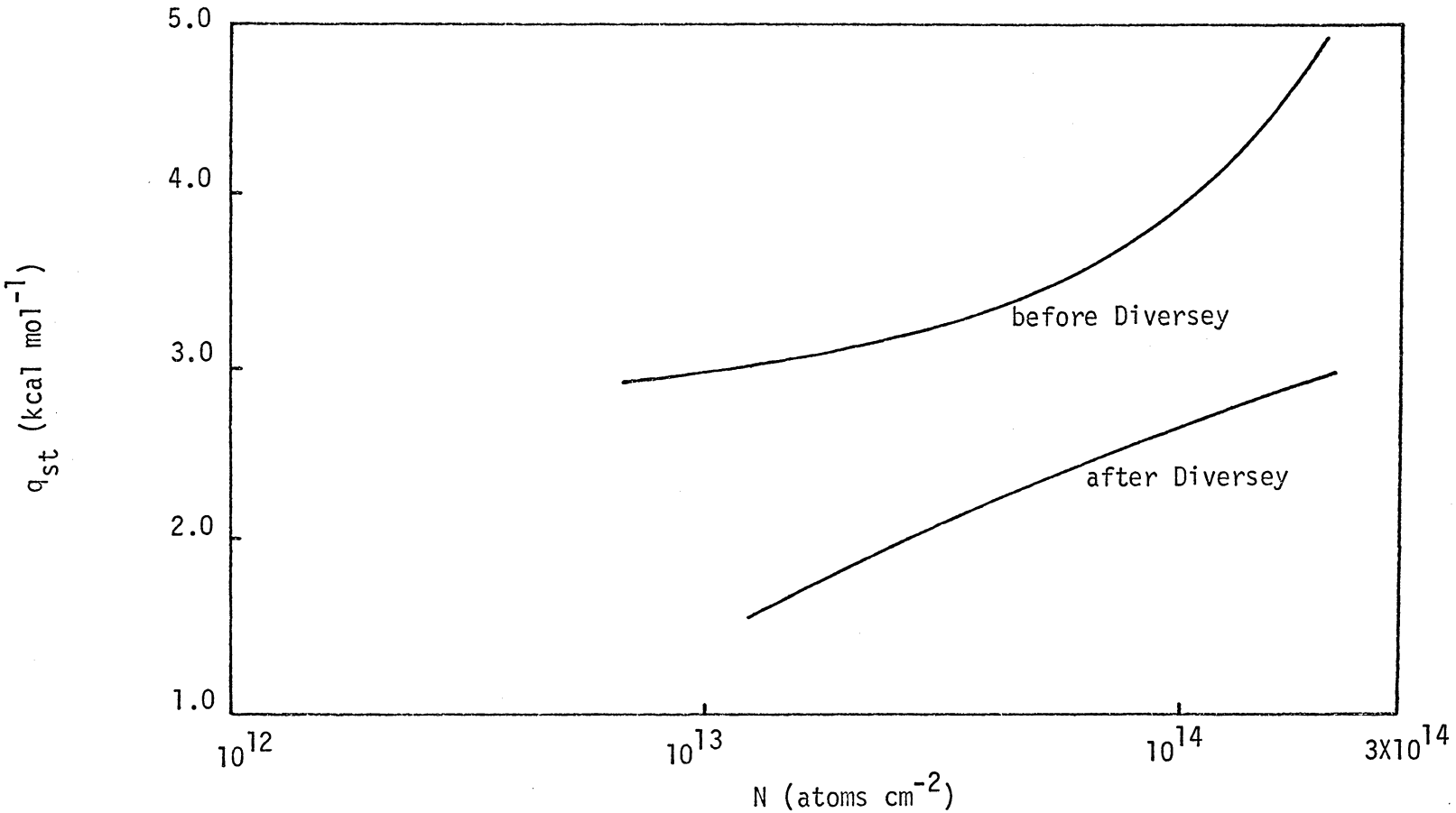

Figure 30. Isosteric heat for krypton on iron.

krypton, and nitrogen were physisorbed on iron, and this question was further studied by work function measurements (see section B).

The D-R plot of nitrogen adsorbed on iron after the Diversey process obtained simultaneously with work function measurements is presented in Figure 31. The D-R line is parallel but lower than the line in Figure 24 where work function measurements were not taken simultaneously. This is good evidence that work function measurements did disturb the adsorbed gas. Presumably, the incident electron flux desorbed the physisorbed nitrogen molecules.

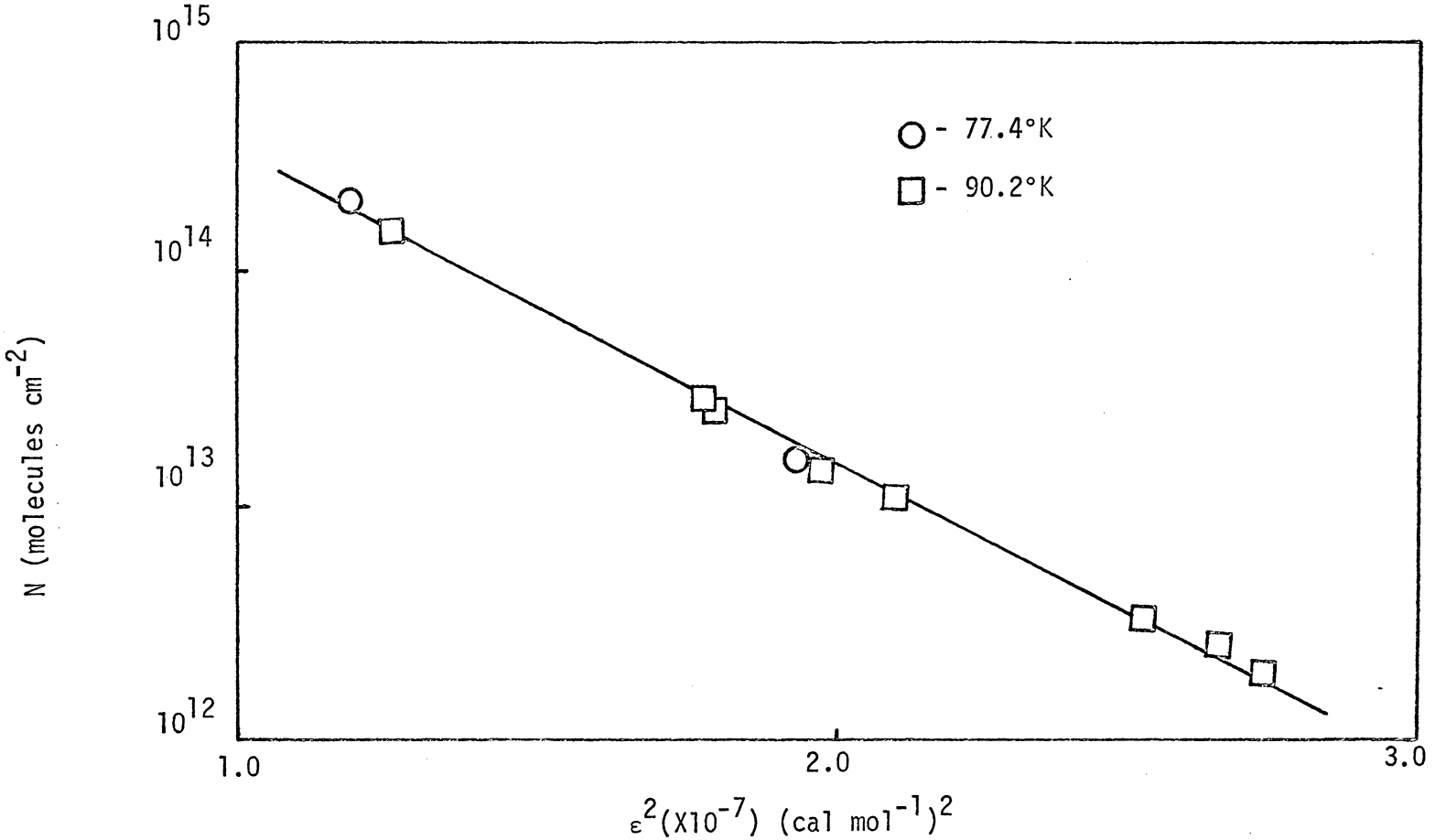

Figure 31. Dubinin-Radushkevich plots for nitrogen on iron after Diversey process and with work function on, by using equations (1) and (13).

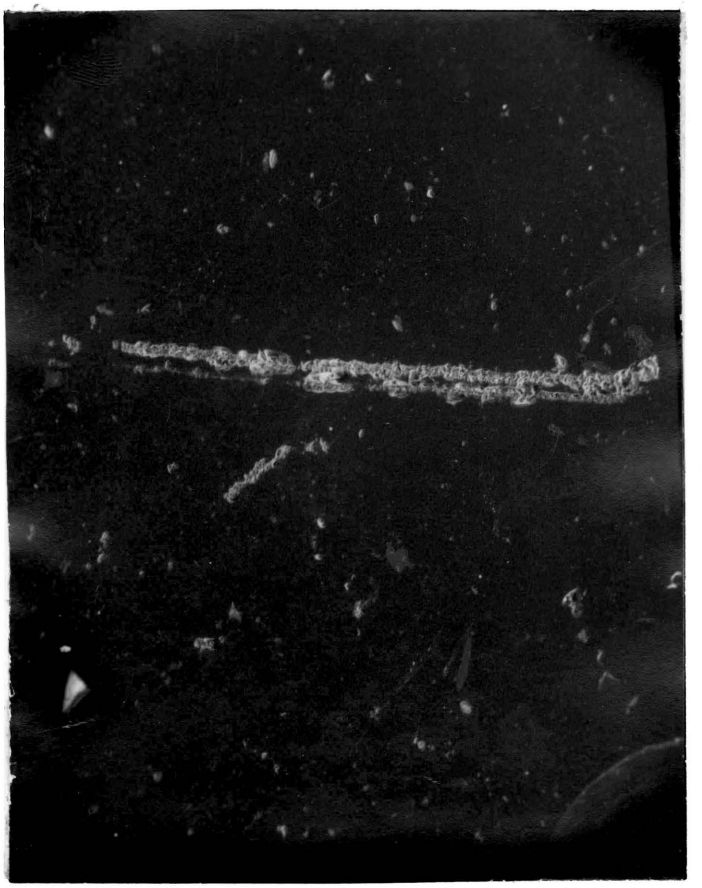

Figure 32. Scanning electron microscopy photomicrograph of the the Pyrex surface (X50).

3. Dubinin-Radushkevich Parameters

A summary of values for the D-R parameter, B, and the limiting (maximum) mean adsorption energy, $(\pi/4)^{\frac{1}{2}}\ (B)^{-\frac{1}{2}}$ obtained by using the modified D-R-P theory is presented in Table II. It is interesting to note that the values of both B and $(\pi/4)^{\frac{1}{2}}\ (B)^{-\frac{1}{2}}$ primarily depend on the adsorbate rather than the adsorbent. For example, the argon/Pyrex and argon/iron systems have B values of 0.590 and 0.563, whereas nitrogen/Pyrex and nitrogen/iron systems have B values of 0.321 and 0.342. Further, the limiting (maximum) mean adsorption energies, $(\pi/4)^{\frac{1}{2}}(B)^{-\frac{1}{2}}$ of argon and krypton are smaller than their corresponding latent heats, q_o, while that of nitrogen is larger.

Values of the D-R parameter, N_m, for all the systems based on the modified D-R-P theory are listed in Table III. For the nitrogen/Pyrex and argon/Pyrex systems, the values in Table III can be compared to the close packed monolayer values of 6.17×10^{14} molecules cm^{-2} for nitrogen and 7.24×10^{14} atoms cm^{-2} for argon. These values were calculated by using cross-sectional areas of nitrogen as 16.2 $\mathring{A}^2$ $molecule^{-1}$ and of argon 13.8 $\mathring{A}^2$ $atom^{-1}$. The agreement is especially good for the case of argon, but is about a factor of 1.3 less than the close packed monolayer value for the case of nitrogen. Hobson and Armstrong[2] reported that their best results were obtained for nitrogen; the value for argon

TABLE II. DUBININ-RADUSHKEVICH PARAMETER, B

System	(T_{o_K})	B (mol kcal^{-1})^2	$(\pi/4)^{\frac{1}{2}}(B)^{-\frac{1}{2}}$ (kcal mol^{-1})	q_o^* (kcal mol^{-1})
N_2/Pyrex	77.4 & 90.2	0.321	1.56	1.51 (S) 1.33 (V)
Ar/Pyre	77.4, 81.8 88.1 & 90.2	0.590	1.15	1.97 (S) 1.53 (V)
Ar/Iron	77.4 & 90.2	0.563	1.18	1.97 (S) 1.53 (V)
N_2/Iron	77.4 & 90.2	0.342	1.52	1.51 (S) 1.33 (V)
Kr/Iron	77.4 & 90.2	0.352	1.49	2.50 (S) 2.31 (V)
Ar/Iron after Diversey	77.4 & 90.2	0.581	1.16	1.97 (S) 1.53 (V)
N_2/Iron after Diversey Process	77.4 & 90.2	0.315	1.58	1.51 (S) 1.33 (V)
Kr/Iron after Diversey Process	77.4 & 90.2	0.365	1.47	2.50 (S) 2.31 (V)
N_2/Iron after Diversey Process and with work function on	77.4 & 90.2	0.311	1.58	1.51 (S) 1.33 (V)

*Latent heats of vaporization (V), and sublimation (S).

TABLE III. DUBININ-RADUSHKEVICH PARAMETER, N_m

Gas / Solids		N_2			Ar			Kr	
		N_m	Ratio		N_m	Ratio		N_m	Ratio
		(mol.cm^{-2})	to A	to B	(atoms cm^{-2})	to A	to B	(atoms cm^{-2})	to B
Pyrex	A	4.66×10^{14}	1		7.44×10^{14}	1			
Iron before Diversey	B	6.40×10^{15}	13.7	1	3.21×10^{16}	40.8	1	4.55×10^{16}	1
Iron after Diversey	C	1.82×10^{16}	39.1	2.85	1.29×10^{17}	173	4.03	1.82×10^{17}	4.01
Iron after Diversey and with work function on	D	8.25×10^{15}	17.7	1.33					

differed by a factor of 8 from the calculated monolayer capacity. However, their results were based on the original D-R-P theory.

The surface area of Pyrex calculated from the extrapolated N_m value for the argon/Pyrex system agreed well with the measured geometric area indicating a very smooth surface. This is consistant well with the generally accepted concept of glass surfaces. A SEM photomicrograph of the Pyrex sample surface is shown if Figure 32 which also shows a smooth surface with some mechanical scratches.

Figures 33, 34 and 35 are the ESCA spectra obtained for the Pyrex surface. Surface carbon contamination is evident in Figure 33, and the presence of sodium and silicon in the surface layer is seen in Figures 34 and 35.

The columns of ratios in Table III represent the relative surface roughness of the adsorbents. The iron surface before the Diversey process had about 40 times the surface area of Pyrex based on the argon data. The iron surface after the Diversey process had about 170 times the surface area of Pyrex. Thus, the Diversey process created about 4 times more iron surface area. SEM photomicrographs of these iron surfaces are shown in Figures 36 and 37. The SEM photomicrograph of the iron surface before the Diversey process shown in Figure 36 indicates a smooth surface with mechanical grinding traces. The photomicrograph of the iron surface after the Diversey process shown in Figure 37 clearly indicates the surface was roughened considerably by using this process.

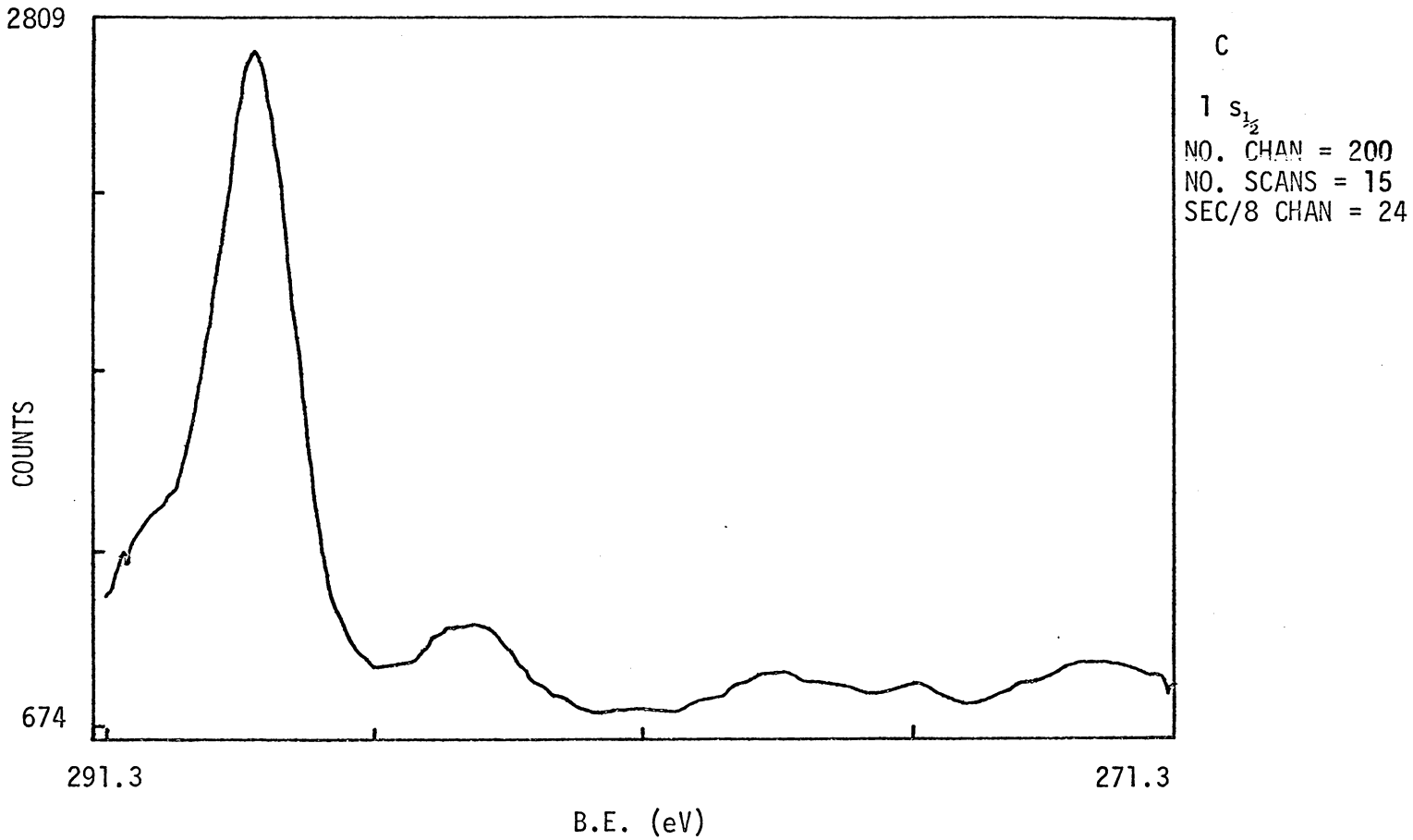

Figure 33. An ESCA spectrum of carbon in Pyrex.

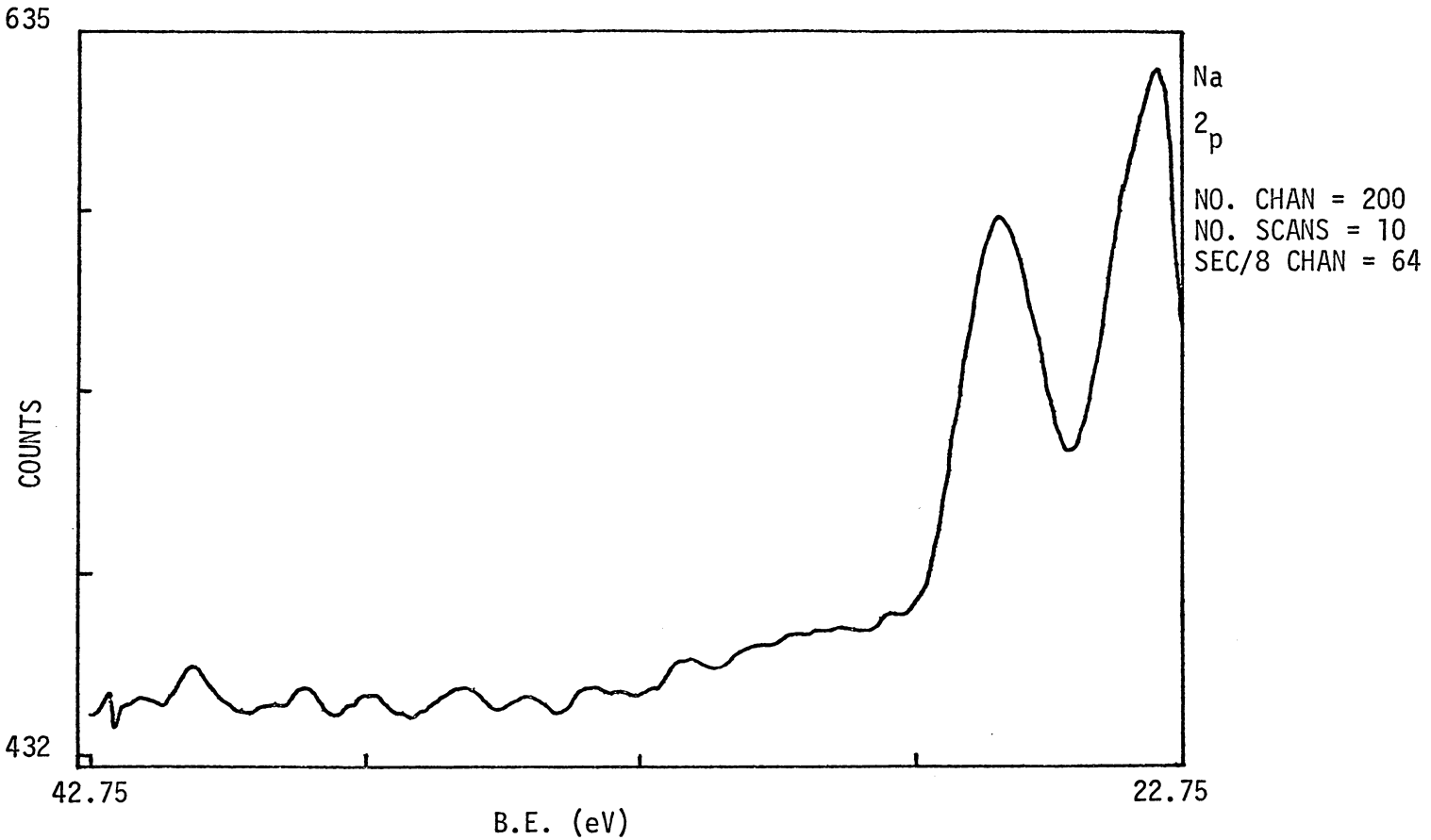

Figure 34. An ESCA spectrum of sodium in Pyrex

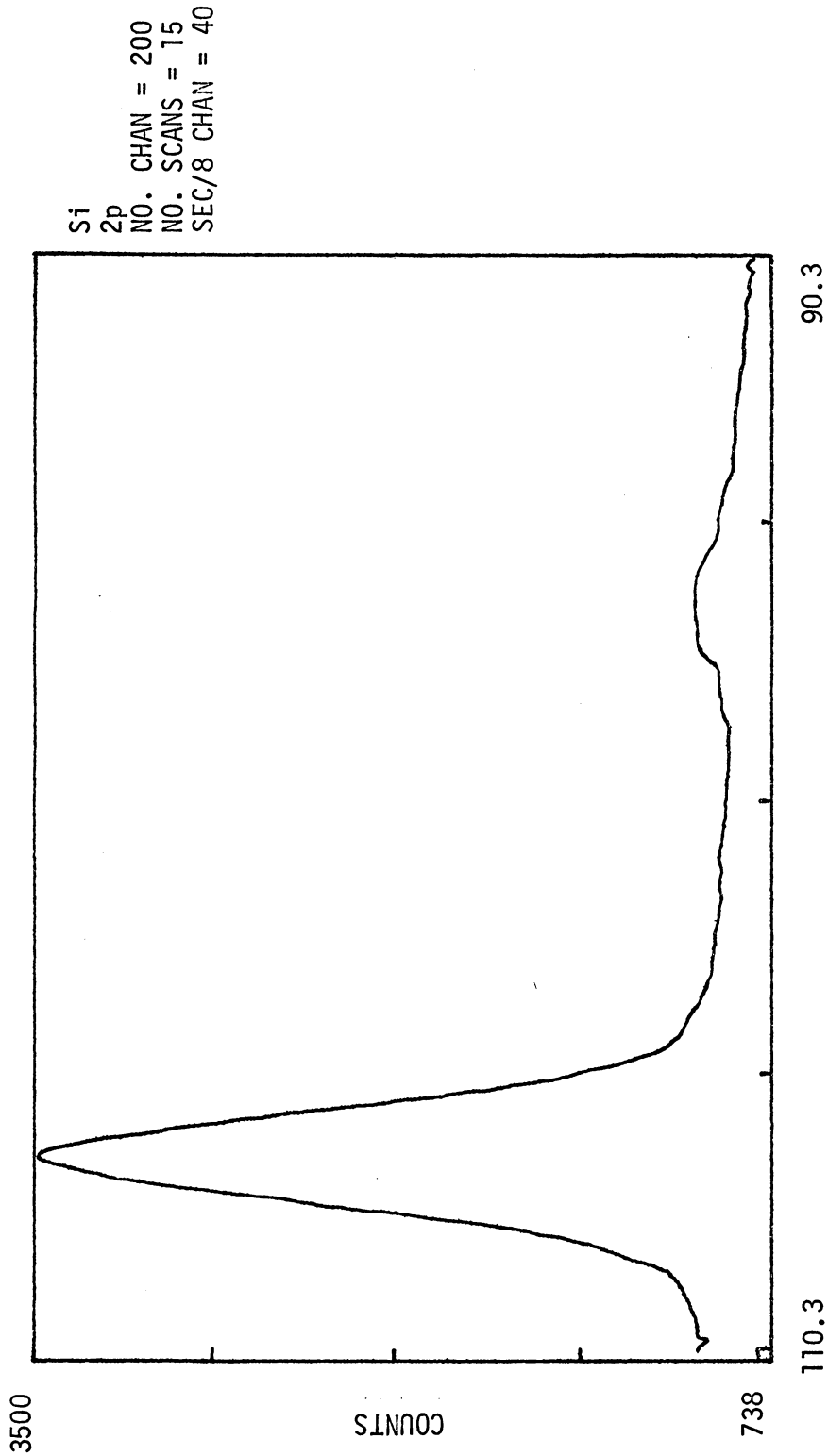

Figure 35. An ESCA spectrum of silicon in Pyrex.

Figure 36. Scanning electron microscopy photomicrograph of iron surface before the Diversey process (X5000).

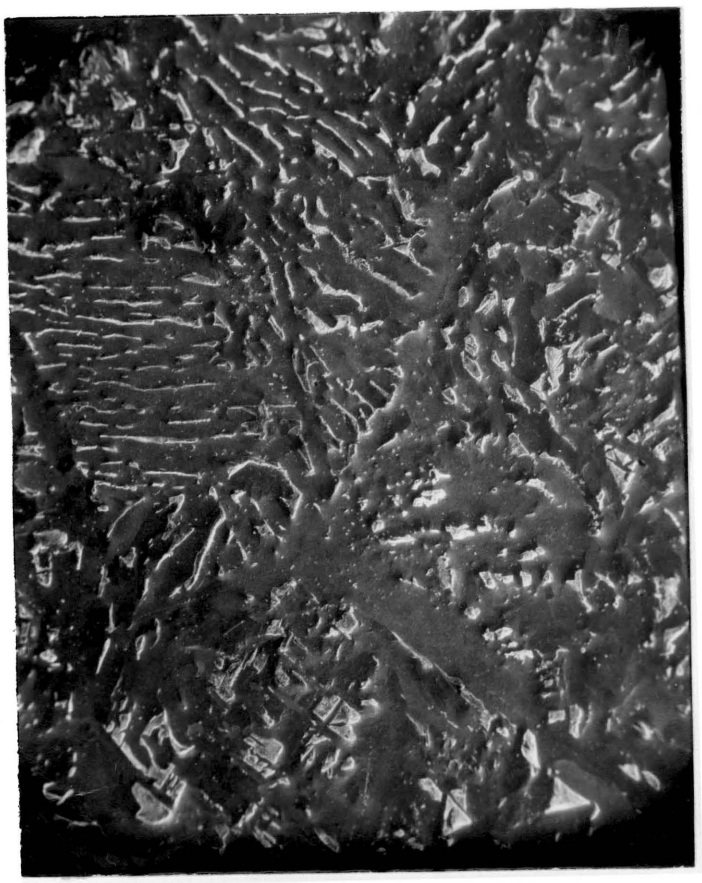

Figure 37. Scanning electron microscopy photomicrograph of the iron surface after the Diversey process (X50).

The ESCA spectra of these two surfaces are shown in Figures 38 and 39. Both spectra indicate the existence of a surface layer of iron oxide as noted by the peak broadening at 716 eV. and the shift to higher binding energy, from 712 to 716 eV. The ion surface after the Diversey process has about the same relative intensity of iron as it had before the cleaning process.

The influence of work function measurements on the adsorption measurements is seen in Table III. About 54.6% of the nitrogen molecules were desorbed by the "hot" electron flux. This is not unexpected since a value of $6X10^{8}$ e cm^{-2} for the incident electron flux was calculated in the Appendix I. If we further consider the energy of the incident electron and the thermal radiation from the hot filament, the above perturbation is even greater. The adsorption of gases on the thoria coated filament was negligible since the filament was hot.

A comparison of limiting (maximum) mean adsorption energy values, $(\pi/4)^{\frac{1}{2}}(B),^{-\frac{1}{2}}$ with the polarizabilities of three adsorbates is given in Table IV. Since argon and krypton are spherical in shape and only interact through dispersion forces, the higher polarizability of krypton certainly made a contribution to the higher value of the limiting mean adsorption energy. For the case of nitrogen, the high value of limiting mean adsorption energy is believed to be due to interactions of its large quadrupole moment with the polar surfaces (quadrupole-dipole interaction).

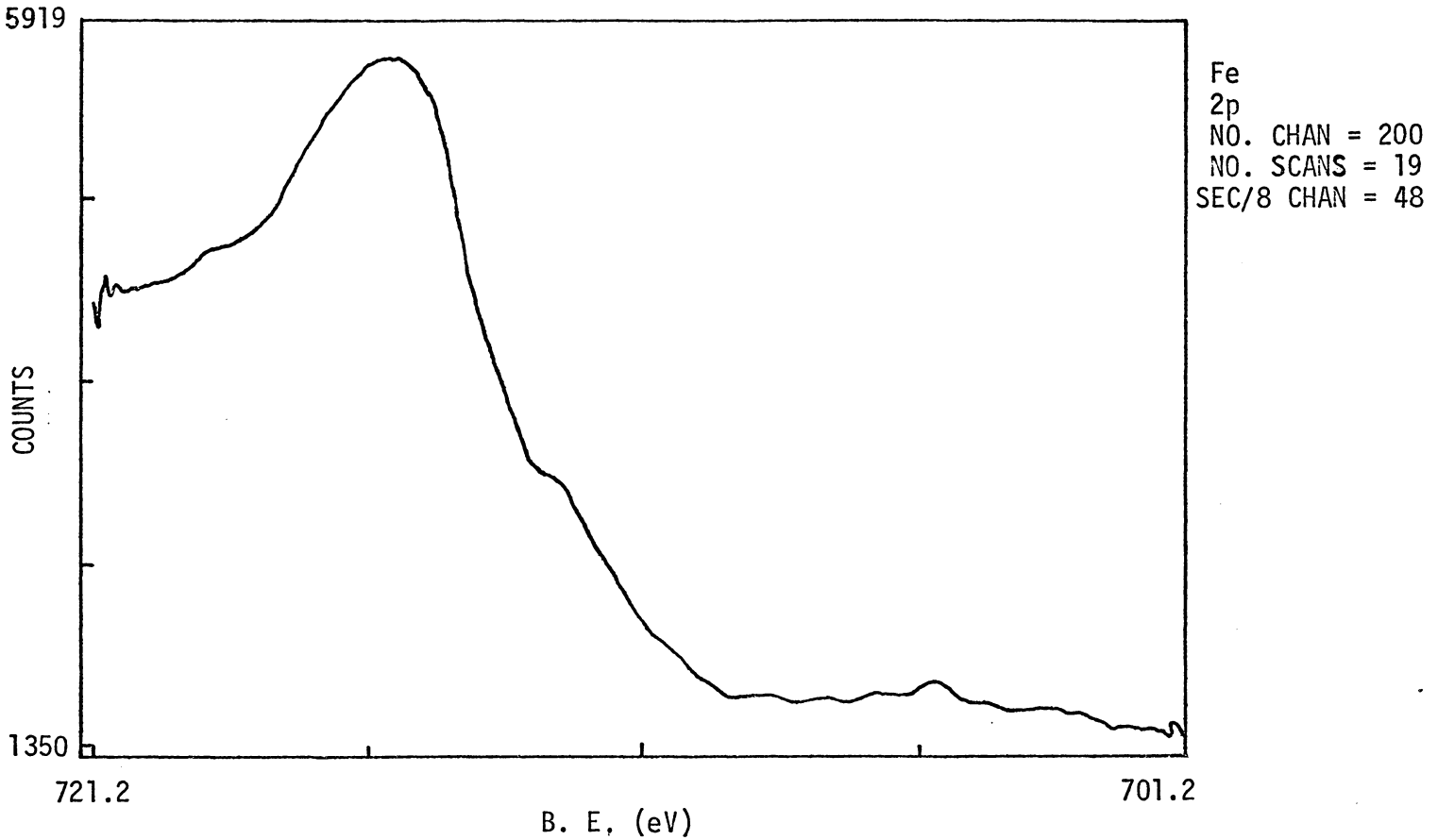

Figure 38. An ESCA spectrum of iron in the iron sample before the Diversey Process.

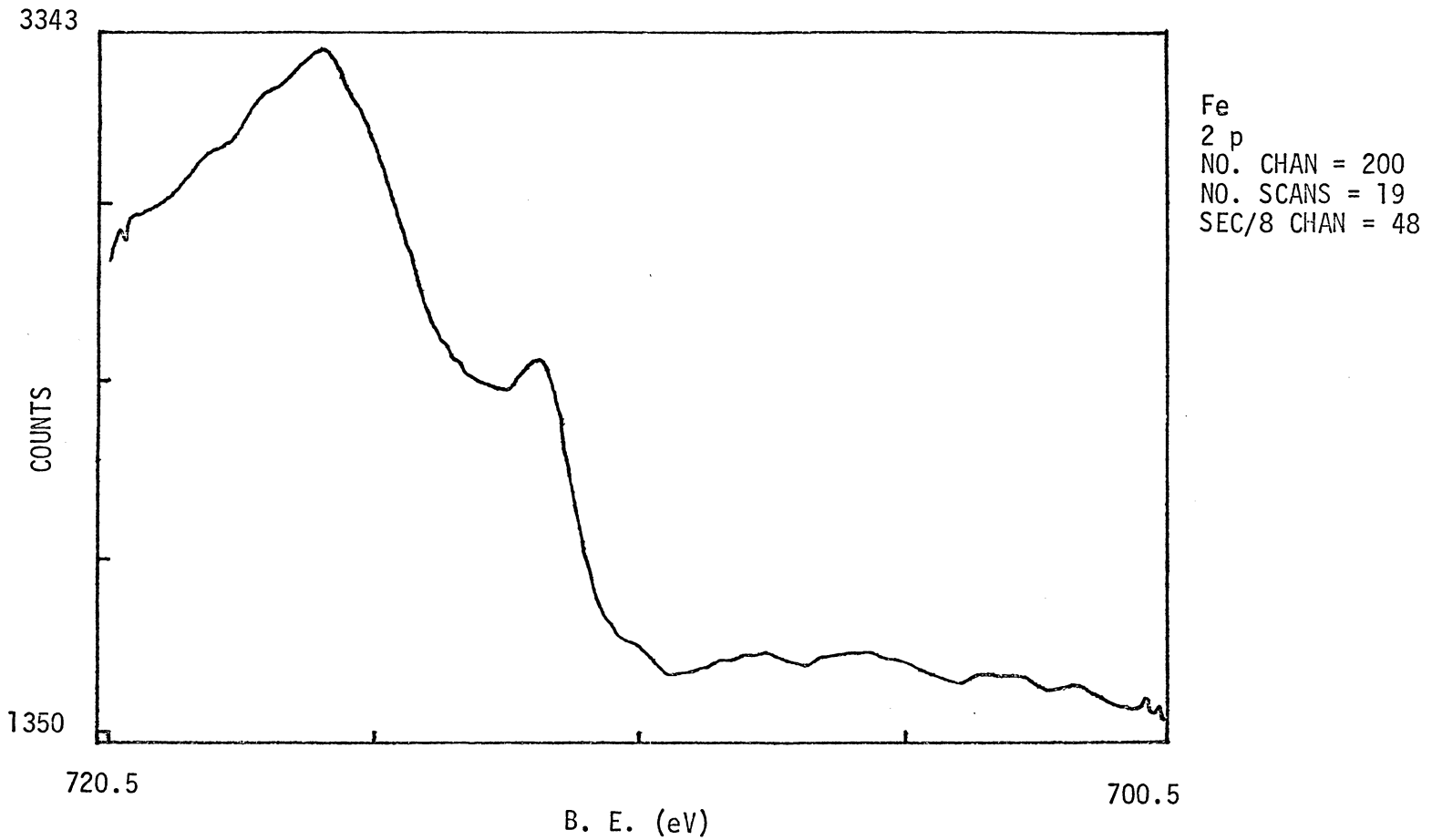

Figure 39. An ESCA spectrum of iron in the iron sample before the Diversey process.

TABLE IV. THE LIMITING (MAXIMUM) MEAN ADSORPTION ENERGIES AND ADSORBATE POLARIZABILITIES.

	$(\pi/4)^{\frac{1}{2}}(B)^{-\frac{1}{2}}$ (kcal mole^{-1})	α (10^{-24} cm^3 mole^{-1})
Ar	1.16	1.63
N_2	1.56	1.71
Kr	1.48	2.47

B. Work Function Measurements

Work function changes were measured for the nitrogen/iron system after the Diversey process while the adsorption isotherm was being measured. The results are given in Table V. Values of the work function change are tabulated as a function of surface coverage, θ. Values of $\Delta \phi$ are all positive which has been interpreted by some authors to mean physisorption took place; however, this point has been questioned.[13] A rather large error of about 40% is associated with the $\Delta \phi$ values, in Table V. The error was due to unstable read-out in part caused by electronic noise and distrubance of the adsorbed layer by the incident electrons. No attempt could be made to use these results in further calculations, such as Equation (19).

C. Contact Angle Measurements

Averaged water contact angles on Pyrex and iron surfaces with different surface treatments are tabulated in Table VI. A finite water contact angle was observed for the Pyrex surface. The value of $22 \pm 3°$ is fairly close to the value of 23° reported by Koranyi and Acs[69] with heat and elapsed time treatments. On the other hand, this value is considerably higher than the values of 4 to 6° obtained by Jen,[68] and by Koranyi and Acs[69] with only heat treatment. This is probably due to contamination of the surface by the ethylene

TABLE V. WORK FUNCTION CHANGES OF NITROGEN ADSORBED ON IRON

T (°K)	Θ	ΔØ (eV)
90.2	0.0002	+0.44
	0.00023	+0.17
	0.00031	+0.26
	0.0004	+0.16
	0.0013	+0.28
77.4	0.00042	+0.28
	0.0016	+0.29
	0.023	+0.28

TABLE VI. WATER CONTACT ANGLES

Solid Surface	Surface Treatment	Mean Value (degree)	Stand. Dev. (degree)	Number of Measurements	Temp. (°C)
Pyrex	$C_2H_4Cl_2$	22	3	82	27
Iron	$C_2H_4Cl_2$	84	3	212	28
Iron	Diversey Process	21	2	22	28
Iron	Diversey Process & set in air for several days	77	5	108	29

dichloride used to wash the Pyrex in the present work. The same argument can be applied to the results of water contact angles on iron washed with ethylene dichloride. In this case, a high water contact angle was also observed.

Iron cleaned with the Diversey process gave considerably lower water contact angles as compared to the results of water contact angles on iron surface treated solely with ethylene dichloride. This reflects the sensitivity of contact angles to surface contamination.

By comparing the last two rows of Table VI, it is clear how seriously the sample surface can be contaminated by ordinary laboratory air. The water contact angle increased from 21 to 77° after the sample was exposed in laboratory air for several days. This type of effect has been commented on infrequently in previous work of this kind.

V. CONCLUSIONS

The following conclusions were based on a study of the adsorption of argon, krypton, and nitrogen on Pyrex and iron in the temperature range from 77.4 to 90.2°K and in the pressure range from 10^{-9} to 10^{-4} torr:

1. The Dubinin-Radushkevich-Polanyi (D-R-P) theory was extended to low pressure adsorption and this modified theory gave better data correlation than the original theory. The modified theory does not specify the state of the adsorbed phase and further the adsorbed phase is a function of the adsorption temperature.

2. No anomalous temperature dependency was found in the D-R lines for any of the five systems studied using the modified D-R-P theory.

3. No evidence was found for non-isothermal conditions in the experimental apparatus in either the nitrogen/Pyrex or the argon/Pyrex systems.

4. The parameter B in the D-R-P theory was found to be dependent primarily on the adsorbate.

5. Argon gave a better surface area measurement on Pyrex than nitrogen. The geometric area of Pyrex was close to its argon surface area. This conclusion was supported by the smooth Pyrex surface observed in the SEM photomicrograph.

6. The surface of iron before and after the Diversey process consisted of an oxide layer based on ESCA analysis.

7. The Pyrex surface was highly heterogeneous while the iron surface both before and after the Diversey process was less heterogeneous, based on calculated isosteric heats of adsorption.

8. Physisorption occurred in all systems based on the magnitude of the calculated isosteric heats of adsorption.

9. The effect of the Diversey process on the iron surface was to increase surface roughness based on adsorption capacity. Photomicrographs of the iron surfaces observed with SEM support this conclusion.

10. The measurement of work function change to monitor the surface of iron during the physisorption of nitrogen was marginal.

11. Water contact angle measurements on both Pyrex and iron were sensitive to contamination. It was demonstrated that ordinary laboratory air rapidly contaminated the solid surfaces. A finite water contact angle on Pyrex was found instead of a zero value which is widely used.

BIBLIOGRAPHY

1. M. Troy, Physical Adsorption of Gases on Stainless Steel at Very Low Pressures, Ph.D. dissertation, Chemistry Department, Virginia Polytechnic Institute and State University, 1970.
2. J. P. Hobson and R. A. Armstrong, J. Phys. Chem., 67, 2000 (1963).
3. F. Ricca, R. Medana, and A. Bellardo, Z. Physik. Chem., 52, 276 (1967).
4. F. Ricca, A. Bellardo, and R. Medana, Ricera Sci., 36, 460 (1966).
5. Y. Tuzi and T. Saito, J. Vac. Sci. Technol., 6, 238 (1960).
6. F. Ricca and A. Bellardo, Z. Physik. Chem., 52, 318 (1967).
7. J. P. Hobson, J. Phys. Chem., 73, 2720 (1969).
8. B. Kindl. E. Negri, and G. F. Cerofolini, Surface Sci., 23, 299 (1970).
9. N. Endow and R. A. Pasternak, J. Vac. Sci. Technol., 3, 196 (1966).
10. A Schram, Nuovo Cimento Suppl., 51, 291 (1967).
11. M. Troy and J. P. Wightman, J. Vac. Sci. Technol., 8, 743 (1971).
12. J. S. Jen and J. P. Wightman, J. Vac. Sci. Technol., 9, 1470 (1972).
13. D. M. Young and A. D. Crowell, Physical Adsorption of Gases, Butterworths, London, 1962.

14. S. Ross and J. P. Olivier, On Physical Adsorption, Interscience, New York, 1964.

15. E. A. Flood, ed., The Solid-Gas Interface, Vol. I and II, Marcel Dekker, New York, 1967.

16. A. W. Adamson, Physical Chemistry of Surfaces, 2nd ed., Interscience, New York, 1967.

17. G. A. Somorjai, Principles of Surface Chemistry, Prentice Hall, Englewood Cliffs, New Jersey, 1972.

18. J. P. Hobson, see ref. 15, ch. 14.

19. J. P. Hobson, Can. J. Phys., 37, 300 (1959).

20. J. P. Hobson, Can. J. Phys., 37, 1105 (1959).

21. M. M. Dubinin and L. V. Radushkevich, Proc. Acad. Sci., USSR, 55, 331 (1947).

22. S. Brunauer, Adsorption of Gases and Vapors, Vol. I., Princeton University Press., Princeton, New Jersey, 1945.

23. M. Polanyi, Vech. dent. phsik. Ges., 16, 1012 (1914).

24. D. N. Misra, Surface Sci., 18, 367 (1969).

25. G. F. Cerofolini, Surface Sci., 24, 391 (1971).

26. M. G. Kaganer, Proc. Acad. Sci., USSR, 116, 251 (1957).

27. F. Ricca and R. Medana, LaRic. Sci., 4, 617 (1967).

28. B. G. Baker and P. G. Fox, Trans. Faraday Soc., 61, 2001 (1965).

29. R. A. Outlaw, Gas-Surface Interactions Occurring on Materials within Ultrahigh Vacuum, Ph.D. dissertation, Materials Engineering Science Department, Virginia Polytechnic Institute

and State University, 1971.

30. R. Haul and B. A. Gottwald, Surface Sci., 4, 334 (1966).

31. D. C. Hayward and B. M. W. Trapnell, Chemisorption, 2nd ed., Butterworths, London, 1964.

32. J. J. F. Scholten, P. Zevietering, J. A. Konvalinka, and J. H. de Boer, Trans. Faraday Soc., 55, 2166 (1956).

33. A. Granville and P. G. Hall, J. Chem. Soc., A, 64 (1968).

34. P. G. Hall and C. J. Hope, J. Chem. Soc., A, 2003 (1970).

35. A. Schram, Suppl. Nuovo Cimento, 5, 309 (1967).

36. B. P. Bering and V. V. Serpinskii, Doklady Akad. Nauk. SSSR, 148, 1331 (1963).

37. N. G. Dovaston, B. McEnaney, and C. J. Weedon, Carbon, 10, 277 (1972).

38. F. A. P. Maggs, Carbon, 10, 113 (1972).

39. L. Berenyi, Z. Phys. Chem., 94, 628 (1920).

40. L. Berenyi, Z. Phys. Chem., 105, 55 (1923).

41. K. M. Nikelaev and M. M. Dubinin, Izv. Akad. Nauk. SSSR, Otd. Khim. Nauk., 1165 (1958).

42. M. M. Dubinin, Russ. J. Phys. Chem., 39, 697 (1965).

43. M. Green, ed., Solid State Surface Science, Marcel Dekker, New York, 1969.

44. M. Kaminsky, Atomic and Ionic Impact Phenomena on Metal Surfaces, Wiley, New York, 1969.

45. J. C. Riviere, see ref. 45, p. 180.

46. A. Eberhagen, Fortschr Physik, 8, 245 (1960).

47. R. V. Culver and F. C. Tompkins, Advan. Catalysis, 11, 67 (1959).

48. W. M. H. Sachlter, Angew Chem. Intern. Ed., 7, 677 (1968).

49. H. Shelton, Phys. Rev., 107, 1553 (1953).

50. B. Gysae and S. Wagener, Z. Physik, 115, 296 (1940).

51. R. V. Culver, J. Pritchard and F. C. Tompkins, Surface Activity, Schulman ed., Vol. 2, Academic Press, New York, 1958.

52. A. G. Knapp, Surface Sci., 34, 289 (1973).

53. D. F. Klemperer and J. C. Snaith, Surface Sci., 28, 209 (1971).

54. D. J. Shaw, Introduction to Colloid and Surface Chemistry, 2nd ed., Butterworths, London, 1970.

55. G. E. P. Elliot and A. C. Riddiford, Recent Progress in Surface Science, Vol. 2, J. F. Danielli, ed., Academic Press, New York, 1964.

56. R. F. Gould, ed., Contact Angle, Wettability and Adhesion, Adv. in Chem. Series 43, American Chemical Society, Washington, D. C., 1964.

57. A. M. Schwartz and A. H. Ellison, Harris Research Lab., NASA Report NAS 3-7104, Washington, D. C., Jan. 1966.

58. C. O. Timmons and W. A. Zisman, J. Phys. Chem., 69, 984 (1965).

59. C. O. Timmons, J. Colloid Interf. Sci., 43, 1 (1973).

60. W. J. Herzberg, J. E. Marian and T. Vermeulen, J. Colloid Interf. Sci., 33, 1964 (1970).

61. Y. Tamai, K. Makuuchi and M. Suzuki, J. Phys. Chem., 71, 4176 (1967).

62. M. K. Bernett and W. A. Zisman, J. Colloid Interf. Sci., 28, 243 (1968).

63. G. E. P. Elliot and A. C. Kiddiford, Nature, n4843, 795 (1962).

64. G. E. P. Elliot and A. C. Riddiford, J. Colloid Interf. Sci., 23, 389 (1967)

65. Y. Tamai and K. Aratani, J. Phys. Chem., 76, 3267 (1972).

66. R. N. Wenzel, Ind. Eng. Chem., 28, 988 (1936).

67. P. Barnal, Acta Chem. Scand., 7, 813 (1953).

68. J. P. Wightman and R. H. Honeycutt, Virginia Polytechnic Institute and State University, NASA contractor report. NAS 1-10646-2 Dec. 1971.

69. G. Koranyi and M. Acs, Acta Chim. Hung., 24, 333 (1960).

70. N. Hansen, Vacuum-techik, 11, 70 (1962).

71. R. C. Little, F. G. Carpenter and V. R. Deitz, J. Chem. Phys., 37, 1896 (1962).

72. C. Neumann, Math. Phys., K24, 49 (1872).

73. O. Reynold, Phil. Trans., 170, 727 (1879).

74. C. Maxwell, Phil. Trans., 170, 731 (1879).

75. J. M. Los and R. R. Ferguson, Trans. Faraday Soc., 48, 730 (1952).

76. F. C. Tompkins and D. E. Wheeler, Trans. Faraday Soc., 29, 1248 (1933).

77. S. Porter, Dis. Faraday Soc., 8, 358 (1950).

78. A. D. Crowell and D. M. Young, Trans. Faraday Soc., 49, 1080 (1953).

79. L. A. Garden, G. L. Kington and W. Laing, Trans. Faraday Soc., 51, 1558 (1953).

80. S. C. Liang, J. Appl. Phys., 22, 148 (1951).

81. S. C. Liang, J. Phys. Chem., 33, 278 (1955).

82. S. C. Liang, J. Phys. Chem., 57, 910 (1953).

83. S. C. Liang, Can. J. Chem., 33, 278 (1955).

84. M. J. Bennett and F. C. Tompkins, Trans. Faraday Soc., 57. 185 (1957).

85. S. Weber, Comm. Kamerlingh. Onnes Lab. Univ. Leiden, 346d, 1 (1936).

86. M. G. I. Sin, J. Vac. Sci. Technol., 10, 368 (1973).

87. C. W. Griffin, Inorganic Quantitative Analysis, 2nd ed., Blakiston, New York, 1949.

88. L. B. Harris, J. B. Hudson and S. Ross, J. Phys. Chem., 71, 377 (1967).

89. M. Troy and J. P. Wightman, J. Vac. Sci. Technol., 7, 429 (1969).

APPENDIX I

CALCULATION OF THE INCIDENT ELECTRON FLUX

In the work function measurements; for a filament courrent of 1.99 A and a dc voltage of 4.00 V, the electron flux current (I) reaching the adsorption vessel (anode) was measured to be $4.21X10^{-11}$ A by using a picoampmeter. Then

$$I = 4.21X10^{-11}\ A$$
$$= 4.21X10^{-11}\ C\ sec^{-1}$$
$$= 4.21X10^{-11}/1.60X10^{-19}\ (C\ sec^{-1})/(C\ e^{-1})$$
$$= 2.63X10^{8}\ e\ sec,^{-1}$$

the geometric area (A) of iron vessel = 1.32 cm^2,

thus,

$$I/A = 2.63X10^{8}/\ 132$$
$$= 1.99X10^{6}\ e\ cm^{-2}\ sec.^{-1}$$

For a 5 minute operation,

$$I/A = 5.97X10^{8}\ e\ cm^{-2}$$

APPENDIX II

PHYSICAL CONSTANTS OF GASES

Gas	M.Wt.	b.p.(°K)	m.p.(°K)	T_c(°K)[1]	P_c(atm)[1]	V_c(ml mol^{-1})[1]	($\AA^2$ $molecule^{-1}$)
N_2	28.0	77.4	63.3	126.0	33.5	90.0	16.2[2]
Ar	39.9	87.5	84.0	151.0	48.0	75.2	13.8[3]
Kr	83.8	120.9	116.6	210.6	54.2	92.0	19.5[4]

(1) W. Kauzman, Kinetic Theory of Gases, Benjamin, N. Y., 1966.

(2) S. Brunauer, P. H. Emmett, and E. Teller, J. Amer. Chem. Soc., 60, 309 (1938)

(3) D. M. Young and A. D. Crowell, Physical Adsorption of Gases, Butterworth, London, 1962.

(4) G. L. Raines Jr. and P. Cannon, J. Phys. Chem., 64, 997 (1960)

APPENDIX III

ERROR ANALYSIS

The uncertainty for a result of F, which was calculated from a set of independent experimentally determined quantities x, y, z,....., can be evaluated by the equation,

$$dF = \left(\frac{\partial F}{\partial x}\right)_{y,z,\ldots} dx + \left(\frac{\partial F}{\partial y}\right)_{x,z\cdots} dy + \ldots\ldots \quad \text{(IV -1)}$$

The relative probable error then can be calculated as

$$\frac{dF}{F} = \left\{ \sum_{n_i} \left[\frac{\left| \left(\frac{\partial F}{\partial n_i}\right) N_{j \neq i} \right| \cdot \left| dn_i \right|}{F} \right]^2 \right\}^{\frac{1}{2}} \quad \text{(IV -2)}$$

Thus, to evaluate the relative probable error of N for the present study, Equation (20) was rewritten as

$$N = \frac{N_o V}{RAT_1} \left[P_1 - GP_2 - (1-G)\, P_2 \left(\frac{T_1}{T_2}\right)^{\frac{1}{2}} \right] \quad \text{(IV -3)}$$

where $G = \frac{V_h}{V}$. Take the derivative of N with respect to each variable and hold the rest constant, then,

$$\frac{\partial N}{\partial P_1} = \frac{N_o \; V}{R \; A \; T_1} \quad \text{(IV -4)}$$

V_h : 478.9 - 577.0 cm^3

A : 128.5 - 237.5 cm^2

And for the adsorption on iron, the experimental variables were within the following ranges;

P_1 : 10^{-8} - 10^{-4} torr

P_2 : 10^{-9} - 10^{-5} torr

T_1 : 295 - 302 °K

T_2 : 77.4 - 90.2 °K

V : 1711.6 cm^3

V_h : 1608.3 cm^3

V_c : 103.3 cm^3

A : 132.4 cm^2

Take the maximum values of the above quantities, and substitute them into the Equations (IV-2) to (IV-10). The relative probable error of N for the adsorption on Pyrex was 5.47% and for the adsorption on iron was 13.2%.

To estimate the relative probable error in ε^2, the following equations were used;

$$\varepsilon^2 = R^2 T^2 \ln^2 \left[\left(\frac{T}{T_c}\right)^2 \left(\frac{P_c}{P}\right) \right]$$

$$\frac{\partial \varepsilon^2}{\partial T} = -2R^2T^2 \ln \left[\left(\frac{T}{T_c}\right)^2 \left(\frac{P_c}{P}\right) \right] + 4R^2T \ln \left[\left(\frac{T}{T_c}\right)^2 \left(\frac{P_c}{P}\right) \right]$$

and

$$\frac{\partial \varepsilon^2}{\partial P} = \frac{2R^2T^2}{P} \ln \left[\left(\frac{T}{T_c}\right)^2 \left(\frac{P_c}{P}\right) \right] \qquad \text{(IV -13)}$$

For argon, the relative probable error was 1.63%. For krypton, the relative probable error was 1.63%. For nitrogen, the relative probable error was 1.77%.

Combining the above errors, the relative probable error of B was <15%. The error in calculating q_{st} was <15%

The same type of calculation was made for the work function study. It was found that the relative probable error was about 40%.

The vita has been removed from the scanned document

PHYSICAL ADSORPTION OF ARGON, KRYPTON, AND NITROGEN ON PYREX AND IRON AT LOW PRESSURES

by

JAMES S. JEN

(ABSTRACT)

Physisorption of argon, krypton, and nitrogen on Pyrex and iron was studied by a static technique in a constant volume system, in the temperature range 77.4 to 90.2°K and in the pressure range 10^{-9} to 10^{-4} torr. Analyses via Electron Spectroscopy for Chemical Analysis (ESCA), Scanning Electron Microscopy (SEM), and Neutron Activation Analysis (NAA) were made to characterize the solid sample surfaces. Both Pyrex and iron surfaces were degreased with ethylene dichloride. The iron surface was further cleaned using the Diversey process. Both surfaces were given a mild bake in vacuum. A modified Dubinin-Radushkevich-Polanyi (D-R-P) theory was used for interpreting the experimental results. This theory assumes that the adsorbed phase is not necessarily liquid-like and is a function of adsorption temperature. Comparisons were made between the modified and the original theories and it was found that the modified theory had a wider applicability and gave better data correlation for all five systems in the present study. It was found that the Dubinin-Radushkevich (D-R) parameter B, and the limiting (maximum) adsorption energy, $(\pi/4)^{\frac{1}{2}}$ $(B),^{-\frac{1}{2}}$ of all systems were primarily dependent on the adsorbate. A correlation between the limiting mean adsorption energy

and the polarizability of adsorbate was made. From the D-R parameter, N_m, it was found that the effect of the Diversey process on iron was to increase the surface area.

Isotherms of the argon/Pyrex system showed that Henry's Law behavior was reached at low coverages and high temperatures. Isosteric heats of adsorption were calculated for all systems. Isosteric heat versus coverage curves indicated that the Pyrex surface was heterogeneous and the iron surface was less heterogeneous. The magnitude of isosteric heats also indicated that all three gases were physisorbed on the Pyrex and iron.

Work function measurements were taken simultaneously with the adsorption isotherm measurements. The results were marginal but confirmed that nitrogen was physisorbed on iron. Water contact angles on Pyrex and iron surfaces were also measured. It was found that the contact angle was very sensitive to the surface contamination and that ordinary laboratory air may contaminate the sample surface very rapidly. A finite water contact angle on Pyrex was found instead of a zero contact angle as is generally used in many works.